Electromagnetic Dissociation Effects in Galactic Heavy-Ion Fragmentation

John W. Norbury and
Lawrence W. Townsend

NASA

Electromagnetic Dissociation Effects in Galactic Heavy-Ion Fragmentation

John W. Norbury

Old Dominion University
Norfolk, Virginia

Lawrence W. Townsend

Langley Research Center
Hampton, Virginia

SUMMARY

Methods for calculating cross sections for the breakup of galactic heavy ions by the Coulomb fields of the interacting nuclei are presented. With the Weizsäcker-Williams method of virtual quanta, estimates of electromagnetic dissociation cross sections for a variety of reactions applicable to galactic cosmic ray shielding studies are presented and compared with other predictions and with available experimental data.

INTRODUCTION

As the Space Station era approaches, concern is mounting over the need to provide adequate protection for astronauts from galactic and solar cosmic rays. Although 98 percent of cosmic radiation consists of particles lighter than lithium (ref. 1), the relativistic nucleus component of galactic cosmic rays will be of major radiobiological significance for extended stays or repeated journeys into space. When interacting with tissue, these relativistic nuclei cause unique biological damage in the form of microlesions (ref. 2). Further, it is known that high LET (linear energy transfer) particles, which compose galactic cosmic rays, are highly carcinogenic, especially for chronic low exposures (ref. 3), and produce residual damage in skin many years after exposure (ref. 4).

In previous work (refs. 5 to 17), a comprehensive nuclear interaction theory capable of describing absorption, total, and fragmentation cross sections at a large variety of energies has been developed for use as input to a radiation transport theory under concurrent development (refs. 18 to 21). This transport theory is needed for reliable analyses of self-shielding factors, as well as for determinations of personal and bulk shielding requirements.

It has recently been found (refs. 22 to 30) that the dissociation of projectile nuclei by the virtual photon field of target nuclei has cross sections which are a sizable fraction of the nuclear projectile fragmentation cross sections. A similar situation also occurs for target fragmentation (ref. 29). Consequently, when comparing a theory with inclusive data, one must include, as a minimum, both the nuclear fragmentation process and the electromagnetic or Coulomb dissociation process. (These two exclusive channels may exhaust the inclusive data; although, in principle, one should consider other possible channels.) Thus, it is of crucial importance when the Coulomb dissociation cross section is a considerable fraction of the inclusive cross section which is true for few-nucleon removal.

In figures 1 through 6 we have presented some simple pictures to help visualize the differences between dissociation due to the nuclear field and dissociation due to the electromagnetic field. Figure 5 shows the virtual photon field of the target nucleus interacting electromagnetically with the projectile to cause projectile excitation (and eventual breakup). Note that this process is exactly analogous to the excitation of light nuclei induced by the electromagnetic field of an electron (fig. 7 and ref. 31), which will be extensively studied at the 4-GeV Continuous Electron Beam Accelerator Facility (CEBAF) to be built in Newport News near the Langley Research Center. In the present investigation, the virtual photon spectrum of a target nucleus interacts with the nucleon constituents in the projectile nucleus, whereas at

CEBAF the virtual photons of an electron will interact with the quark constituents of nucleons and nuclei. The energy of the virtual photons causing nuclear dissociation is typically on the order of 20 MeV, whereas the virtual photons at CEBAF will have energies up to 4 GeV (ref. 31).

Because of the importance of nuclear electromagnetic dissociation, it is of great use to supplement the previously developed nuclear fragmentation theory (refs. 5 to 17) with calculations of the Coulomb dissociation cross section. Thus the present report represents an initial effort at estimating Coulomb dissociation cross sections. Given such a beginning effort, the methods employed here are rather simplistic and the resultant cross sections should be considered only as reasonable estimates. Specific suggestions are made as to how to improve future calculations.

The total photodissociation cross section for removal of a particular species X is designated as $\sigma_{EM}(X)$. The symbol X corresponds to that defined in reference 17 as the ablated particle in nuclear fragmentation. In general, photons, neutrons, deuterons, tritons, alphas, dineutrons, and so forth, will decay from a photo-excited nucleus; however, for the present work X is considered to be protons and neutrons only (i.e., one-nucleon removal). The cross section is evaluated (ref. 27) as

$$\sigma_{EM}(X) = \int_{E_o(X)} \sigma_\nu(E,X) \, N(E) \, dE \tag{1}$$

where $E_o(X)$ is the photonuclear threshold which actually depends on X, $\sigma_\nu(E,X)$ is the total photonuclear reaction cross section for production of X, and $N(E)$ is the virtual photon number spectrum. The calculation of $N(E)$ and $\sigma_\nu(E,X)$ is now considered. The symbols used in this paper are defined on pages 18 through 20.

VIRTUAL PHOTON NUMBER SPECTRUM

The classic Weizsäcker-Williams (WW) method of virtual quanta (ref. 32) is used in this report. (Short discussions of this method appear in refs. 33 and 34.) Jackson (ref. 35) has an excellent account of this method and it is Jackson's treatment that we follow. Before proceeding, however, note that an alternative treatment for calculating the virtual photon spectrum of a nucleus has been presented by Jäckle and Pilkuhn (JP) and appears in references 22, 24, and 25. The advantage of the JP method is that it predicts virtual photon spectra for individual multipoles, such as E1 and M1, whereas the WW method does not. Furthermore, the JP method accounts for the finite extent of the charge distribution, whereas the WW method assumes a point charge. Olson et al. (ref. 28) provide a very clear and presentable discussion of the differences between the WW and the JP spectra. They note that the discrepancy between these two methods is not understood and must certainly be resolved if further progress is to be made in this area. The minimum impact parameter b_{min} used in calculation of the virtual photon spectra is given by

$$b_{min} = R_{0.1}(P) + R_{0.1}(T) - d \tag{2}$$

where $R_{0.1}(P)$ and $R_{0.1}(T)$ are the 10-percent-charge density radii of the projectile and target nuclei, respectively (refs. 26 through 28) and d is the overlap

distance treated as an arbitrary parameter. Olson et al. (ref. 28) find good agreement with experimentally determined electromagnetic dissociation cross sections by setting d equal to 1.5 fm for the JP spectrum and to -1.5 fm for the WW spectrum. In fact with these values of d, one finds from table IV of reference 28 that the WW predictions are just as accurate, if not slightly better, than the JP prediction. The very similar results of these two methods is the reason for using the WW method in the present work. However, if one wishes to use the JP method, it is a simple matter to substitute the WW spectrum for the JP spectrum given on page 1531 of reference 28.

The WW virtual photon number spectrum is given by

$$N(E) = \frac{1}{E} \frac{2}{\pi} z_t^2 \alpha \frac{1}{\beta^2} \left\{ x K_0(x) K_1(x) - \frac{1}{2} \beta^2 \left[K_1^2(x) - K_0^2(x) \right] \right\} \tag{3}$$

where $N(E)$ is the number of virtual photons per unit energy E, z_t is the number of protons in the target nucleus, β is the velocity of the target in units of c, and α is the electromagnetic five structure constant given by

$$\alpha = \frac{e^2}{\hbar c} \tag{4}$$

and the parameter x in equation (3) is defined as

$$x = \frac{E b_{min}}{\gamma \beta (\hbar c)} \tag{5}$$

where γ is the usual relativistic factor, and $K_0(x)$ and $K_1(x)$ are modified Bessel functions of the second kind (refs. 36 and 37). The relation between the frequency spectrum dI/dE and the number spectrum is simply (ref. 35)

$$N(E) = \frac{1}{E} \frac{dI}{dE} \tag{6}$$

The frequency and number spectra are shown in figures 8 and 9 and are seen to be comparable to figure 15.8 of Jackson (ref. 35) and figure 2(a) of Olson et al. (ref. 28), respectively.

As a minor technical point concerning evaluation of the Bessel functions, a general analytic expression for them does not exist. Jackson (ref. 35) does provide approximate expressions for them in both the low and high frequency limits; however, in the present applications, these limits are not generally applicable and Jackson's approximations fail badly. Thus, the very good polynomial approximations of Abramowitz and Stegun (ref. 37, pp. 378-379) are actually used here to reliably calculate the spectra for any frequency.

In principle, one should really use the experimentally determined photonuclear reaction cross sections, as in reference 28. (Two excellent reviews of photonuclear reactions are given in refs. 38 and 39.) For the sake of both simplicity and generality, however, the present work uses the parameterization of the total photo-absorption cross section σ_{abs} as developed by Westfall et al. (ref. 27). The branching ratio g_X is defined by

$$\sigma_\nu(E,X) = g_X \, \sigma_{abs}(E) \tag{7}$$

and g_X will be taken from experiment. Following Westfall et al. (ref. 27), it is assumed that σ_{abs} is dominated by the electric giant dipole resonance (E1 GDR) (refs. 38 through 42) so that the present work will take σ_{abs} to be the E1 GDR absorption cross section. (This would only be approximately true (refs. 38 and 39) if one actually used experimental cross sections.) The absorption cross section is therefore given by (ref. 27)

$$\sigma_{abs}(E) = \frac{\sigma_m}{1 + \left[(E^2 - E_{GDR}^2)^2 / E^2\Gamma^2\right]} \tag{8}$$

where E_{GDR} is the energy of the peak in the GDR cross section, Γ is the width of the E1 GDR, and

$$\sigma_m = \frac{\sigma_{TRK}}{\pi\Gamma/2} \tag{9}$$

with the Thomas-Reiche-Kuhn cross section (ref. 43) given by

$$\sigma_{TRK} = \frac{60 N_t Z_t}{A_t} \text{ MeV-mb} \tag{10}$$

where N_t and A_t are the target neutron and mass numbers. The GDR energy is given by (ref. 27)

$$E_{GDR} = \frac{\hbar c}{\left[\dfrac{m^*c^2 R_o^2}{8J}\left(1 + u - \dfrac{1 + \varepsilon + 3u}{1 + \varepsilon + u}\varepsilon\right)\right]^{1/2}} \tag{11}$$

4

with

$$u = \frac{3J}{Q'} A_t^{-1/3} \qquad (12)$$

and

$$R_o = r_o A_t^{1/3} \qquad (13)$$

where $\varepsilon = 0.0768$, $Q' = 17$ MeV, $J = 36.8$ MeV, $r_o = 1.18$ fm, and m^* is $7/10$ of the nucleon mass. The main uncertainties in this cross section are the values of the branching ratios g_x and the width Γ, which can vary from 3 to 10 MeV. The widths Γ are smallest for closed shell nuclei and largest for nonspherical nuclei (ref. 38). Attempts to parameterize Γ have not been very successful (ref. 39). Similarly for the branching ratios, where calculation, for instance, may involve knowledge of direct and statistical components as well as energy level densities of neighboring nuclei (refs. 40 through 42).

Because of the uncertainties in the widths and branching ratios we have performed a detailed study by comparing theoretical cross sections with experiment as presented in figures 10 through 22. The aim of this comparison to experiment was to try to formulate an overall prescription (method) for determining Γ and g_x which could be applied to systems where data do not exist. In figures 10 through 13, we present data and calculations for (γ,n) reactions on ^{12}C, ^{16}O, ^{28}Si, and ^{58}Ni. The widths fitted were 8 MeV for ^{12}C and 10 MeV for the other three nuclei. A branching ratio $g_n = 0.5$ (suggested from equation (A7) of Westfall et al. (ref. 27)) was found to be sufficient. For the (γ,n) reactions on ^{90}Zr, ^{160}Gd, ^{197}Au, and ^{208}Pb (figs. 14 through 17), the widths given in figure 46 of Berman and Fultz (ref. 39) were sufficient as were branching ratios obtained from Weinstock and Halpern (ref. 44) again suggested from equation (A7) of Westfall et al. (ref. 27). For $^{238}U(\gamma,n)$ a fit of $\Gamma = 5$ MeV was required (fig. 18).

These isotopes all have a large relative abundance and we have found a general variation of the width with mass number also in accord with Berman and Fultz (ref. 39). (Note however that fig. 46 of ref. 39 is only appropriate for heavier nuclei which have GDR energies below a value of 18 MeV. Lighter nuclei, such as ^{16}O, have values above this.) Thus, for naturally abundant isotopes, we feel it is safe to interpolate and use width values appropriate to certain mass regions as found in figures 10 through 18; this is done in table 1.

The branching ratios in figures 10 through 18 are all described by what shall henceforth be called the branching ratio equations (BRE) defined as

$$g_p = \text{Min}\left(\frac{Z_p}{A_p}, WH\right) \qquad (14)$$

and

$$g_n = 1 - g_p$$

where equation (14) refers to the minimum value of either Z_p/A_p or the value given by Weinstock and Halpern in reference 44 (denoted as WH in eq. (14)). The BRE is suggested from equation (A7) of Westfall et al. (ref. 27) but note that their equation is only valid in the Fe region. The BRE fits the data in figures 10 through 18 very well.

We warn, however, that these prescriptions for the width and branching ratios are not appropriate for "nonabundant" nuclei such as ^{18}O and ^{54}Fe as shown in figures 19 through 22 where both (γ,n) and (γ,p) cross sections are given. (Experimental data for these figures are from refs. 45 and 42.) Clearly the widths are abnormal (to be suspected from ideas of the shell model) and the fitted branching ratios are quite different to those given by the BRE. The latter point should be obvious. Clearly ^{18}O would prefer to decay through neutron emission and ^{54}Fe through proton emission.

To summarize this comparison with the data (table 1) for "abundant" nuclei, values of Γ can be obtained from neighboring nuclei, and branching ratios can be determined from the BRE. For "nonabundant" nuclei, values must be obtained directly from experiment.

This prescription is followed for the calculations for ^{20}Ne, ^{40}Ar, ^{40}Ca, ^{56}Fe, ^{64}Cu, and ^{108}Ag presented in figures 23 through 28. These nuclei were chosen for present and future calculations of electromagnetic dissociation cross sections. Variations of the photoreaction cross sections with width Γ are shown in figures 23 through 28. The actual values to be used in calculations are given in table 1 and follow the prescription of the preceding paragraph.

Finally, in retrospect, one sees that the theory presented here for calculating (γ,n) and (γ,p) cross sections fits extremely well with the data (figs. 10 through 18), given the very large mass range considered.

ELECTROMAGNETIC DISSOCIATION CROSS SECTIONS

As noted by Olson et al. (ref. 28), the product of the number spectrum with the photoreaction cross section forms a differential electromagnetic dissociation cross section. This cross section can be defined as

$$\frac{d\sigma_{EM}(X,E)}{dE} = \sigma_2(E,X)\, N(E)$$

6

This differential cross section is finally integrated, as prescribed in equation (1), to produce the total electromagnetic dissociation cross section. Note that because g_X is assumed to be energy independent, we can also write

$$\sigma_{EM}(X) = g_X \int_{E_o(X)} \sigma_{abs}(E) \; N(E) \; dE$$

$$= g_X \; \sigma_{EM-abs}(X)$$

with

$$\sigma_{EM-abs}(X) = \int_{E_o(X)} \sigma_{abs}(E) \; N(E) \; dE \qquad (15)$$

being the electromagnetic absorption cross section not to be confused with the photonuclear absorption cross section $\sigma_{abs}(E)$.

As input to the calculations, one needs the proton and neutron threshold energies $E_o(p)$ and $E_o(n)$ as discussed in appendix A and listed in table 2. One also needs the 10-percent-charge radii discussed in appendix B and listed in table 3. The complete computer code listing with sample output is listed in appendix C.

Finally one calculates the electromagnetic dissociation cross sections as listed in tables 4 through 7. The total (proton plus neutron) absorption cross sections for ^{56}Fe at 1.88 GeV/N are given in table 4 for both $d = -1.5$ and 0 fm (see eq. (2)) and compared with the calculations of Westfall et al. (ref. 27) who assumed $d = 0$. The reason that the present values are slightly larger than those of reference 27 is because they used a slightly smaller relativistic factor γ to account for slowing down of the projectile in the target material. In table 5, comparisons are made with experimental values for ^{12}C and ^{16}O incident upon various targets (ref. 26). Overall, one finds outstanding agreement between theory and experiment. Further, both values of d give comparable results.

Unfortunately such is not the case for ^{18}O as shown in table 6. The value of $g_p = 0.4$ obtained by use of figures 19 and 20 is good but is better replaced by $g_p = 0.2$ for $d = -1.5$ fm and by $g_p = 0.3$ for $d = 0$ fm. The unusual structure in the ^{18}O(γ,n) cross section (fig. 20) may account for this discrepancy.

Target fragmentation of ^{197}Au has also been studied as shown in table 7. Here again agreement is not as good as one would like, although the agreement is reasonable and better for $d = 0$ fm.

In conclusion, we have been able to obtain reasonable agreement with a wide range of experimental results. It is suggested that a value of $d = 0$ fm be used in present and future studies. Table 8 provides a compilation of electromagnetic dissociation cross sections for use in a general fragmentation theory. Note that the cross section for ^{238}U on heavy targets is enormous. In order to improve the Coulomb dissociation theory, the most significant advance would be to always use the experimental photonuclear cross sections (both photoneutron and photoproton) rather than

calculating them as done herein. The present work has only considered neutron and proton removal. It would be very useful to have cross sections also for few-nucleon removal such as deuterons, tritons, alphas, diprotons, and dineutrons. Again experimental cross sections would be best to use. Concerning the frequency spectrum, it should be decided whether the WW or the JP spectrum should be used (or some other form) and finally the most correct value of d should be determined.

CONCLUDING REMARKS

Methods for calculating cross sections for the breakup of galactic heavy ions by the Coulomb fields of the interacting nuclei are presented. By using the Weizsäcker-Williams method of virtual quanta, estimates of electromagnetic dissociation cross sections for a variety of reactions applicable to galactic cosmic ray shielding studies are presented and compared with other predictions and with available experimental data.

NASA Langley Research Center
Hampton, VA 23665-5225
November 15, 1985

THRESHOLD ENERGIES

For the reaction

$$M_p + M_t \rightarrow M_3 + M_4 \tag{A1}$$

where M_p and M_t refer to the projectile and target masses, respectively, the projectile threshold kinetic energy for production of M_3 and M_4 is given by

$$T_{th} = \frac{(M_3 + M_4)^2 - (M_p + M_t)^2}{2M_t} \tag{A2}$$

Defining the Q-value as

$$Q = (M_p + M_t) - (M_3 + M_4) \tag{A3}$$

equation (A2) may be written as

$$T_{th} = \frac{-Q(M_p + M_t + M_3 + M_4)}{2M_t} \tag{A4}$$

For photonuclear reactions

$$M_p = 0 \tag{A5}$$

and, therefore, for reactions like $^{54}Fe(\gamma,n)$ and $^{32}S(\gamma,d)$,

$$T_{th} = -Q \tag{A6}$$

to a very good approximation. Note that Q is always negative for reactions because all reactions are endothermic, whereas decays, being exothermic, have positive values of Q.

For more bodies in the final state, such as

$$M_p + M_t \rightarrow M_3 + M_4 + M_5 + M_6 + \ldots + M_N \tag{A7}$$

we simply have

$$T_{th} = \frac{(M_3 + M_4 + M_5 + M_6 + \ldots + M_N)^2 - (M_p + M_t)^2}{2M_t}$$

$$= \frac{-Q(M_p + M_t + M_3 + M_4 + M_5 + \ldots + M_N)}{2M_t} \tag{A8}$$

APPENDIX B

10-PERCENT-CHARGE DENSITY RADII

As input to the electromagnetic dissociation cross sections one requires the 10-percent-charge density radii. De Jager et al. (ref. 46) list half-density radii (C) and diffuseness (z) parameters for input to density parameterizations. The parameterizations considered herein are the Harmonic-oscillator (HO) model,

$$\rho(r) = \rho_o[1 + z(r/C)^2] \exp[-(r/C)^2] \tag{B1}$$

the 2-parameter Fermi (2pF) model,

$$\rho(r) = \frac{\rho_o}{1 + \exp[(r - C)/z]} \tag{B2}$$

the 3-parameter Fermi (3pF) model,

$$\rho(r) = \frac{\rho_o[1 + w(r^2/C^2)]}{1 + \exp[(r - C)/z]} \tag{B3}$$

and the 3-parameter Gaussian (3pG) model

$$\rho(r) = \frac{\rho_o[1 + w(r^2/C^2)]}{1 + \exp(r^2 - C^2)/z^2} \tag{B4}$$

For the 2pF model one can calculate the 10-percent-charge density radius by

$$R_{0.1} = C + 2.2z \tag{B5}$$

However, such a simple analytic form is not available for the other models. Thus, the general method was simply to plot the various densities and determine $R_{0.1}$ graphically. Resultant values are listed in table 3.

11

APPENDIX C

COMPUTER CODE

A computer program which calculates total electromagnetic dissociation cross sections for neutron and proton removal is given in this appendix. Required as input are the mass excesses of the nucleus $^A Z$ in question and also the mass excesses of ^{A-1}Z and $^{A-1}(Z - 1)$ in order to calculate proton and neutron thresholds. Further, the 10-percent-charge density radii, the GDR width, and the proton branching ratio are also required. Other inputs such as proton and mass numbers should cause no problem. At the end of the program is included a sample output.

```
10      REM                 COULOM
20      REM                 ------
30      REM                 ------
40      REM
50                                          FIXED 2
60      REM
70      REM
80      REM         NUMERICAL INTEGRATION WILL BE PERFORMED USING THE TRAPEZOIDAL RULE
90      REM
100     REM
110                 DIM Ephoton(900)
120                 DIM Sigmanu(900)
130                 DIM Ne(900)
140     REM
150     REM
160     REM Fsc = Fine Structure Constant
170     Fsc=1/137.03604
180     Hbarc=197.32858
190     Mncsq=938.95
200     Mneutron=939.5731
210     Mproton=938.2796
220     Amu=931.5016
230     Mstar=.7*Mncsq
240     J=36.8
250     Q=17
260     Epsilon=.0768
270     INPUT "ENTER GDR WIDTH (MeV)",Width
280     INPUT "ENTER Z OF TARGET",Zt
290     INPUT "ENTER A OF TARGET",At
300     Nt=At-Zt
310     INPUT "ENTER Z OF PROJECTILE",Zp
320     INPUT "ENTER A OF PROJECTILE",Ap
330     Np=Ap-Zp
340     INPUT "INPUT PROTON BRANCHING RATIO",Fracproton
350     INPUT "INPUT 10 percent CHARGE DENSITY RADIUS OF TARGET   (fm)",R10t
360     INPUT "INPUT 10 percent CHARGE DENSITY RADIUS OF PROJECTILE   (fm)",R10p
370     INPUT "INPUT Dee  (overlap distance)  (fm)",Dee
380         Bmin=R10t+R10p-Dee
390             INPUT "INPUT MASS EXCESS OF PROJ (MEV) : use correct sign",Mexcessp
400             PRINT "(gamma,n) REACTION HAS NUCLEUS IN FINAL STATE WITH   Z = ",Zp
410             PRINT "(gamma,n) REACTION HAS NUCLEUS IN FINAL STATE WITH   A = ",Ap-
1
420             PRINT
430             PRINT "(gamma,p) REACTION HAS NUCLEUS IN FINAL STATE WITH   Z = ",Zp-
1
440             PRINT "(gamma,p) REACTION HAS NUCLEUS IN FINAL STATE WITH   A = ",Ap-
1
450             PRINT
460             PRINT
470             PRINT
480             INPUT "INPUT MASS EXCESS OF FINAL NUCLEUS FOR (gamma,n) REACTION (ME
V) ",Mexcessgn
490             INPUT "INPUT MASS EXCESS OF FINAL NUCLEUS FOR (gamma,p) REACTION (ME
V) ",Mexcessgp
500             Mproj=Mexcessp+Ap*Amu
510             Mfingn=Mexcessgn+(Ap-1)*Amu
520             Mfingp=Mexcessgp+(Ap-1)*Amu
530             Ethreshgn=((Mfingn+Mneutron)^2-Mproj^2)/(2*Mproj)
540             Ethreshgp=((Mfingp+Mproton)^2-Mproj^2)/(2*Mproj)
550     INPUT "WHAT IS KE/N OF PROJECTILE   (MeV/N) ?",Tlab
560     Gamma=1+Tlab/Mncsq
570     Vel=SQR(1-1/Gamma^2)
580         REM Gamma IS THE RELATIVISTIC GAMMA FACTOR OF PROJ
590         REM Vel   IS VELOCITY OF PROJ IN UNITS OF C  (RELATIVISTIC BETA FACTOR)
600     Sigmam=120*Np*Zp/(PI*Ap*Width)
610     Ro=1.18*Ap^(1/3)
```

```
620    U=3*J*Ap^(-1/3)/Q
630    Egdr=SQR(8.0*J*Hbarc^2/(Mstar*Ro^2)*1./(1+U-(1.+Epsilon+3*U)*Epsilon/(1+Epsi
lon+U)))
640    REM
650    REM      NUMERICAL INTEGRATION OR PLOT
660    REM
670    PRINT "neutron THRESHOLD ENERGY IS   (MeV)",Ethreshgn
680    PRINT
690    PRINT "proton THRESHOLD ENERGY IS   (MeV)",Ethreshgp
700    PRINT
710    PRINT
720         IF Ethreshgn<Ethreshgp THEN Ephoton(1)=Ethreshgn
730         IF Ethreshgn>Ethreshgp THEN Ephoton(1)=Ethreshgp
740    INPUT "ENTER ENERGY UPPER LIMIT FOR NUMERICAL INTEGRATION OR PLOT (MeV)",E
photonmax
750    INPUT "ENTER NUMBER OF INTEGRATION OR PLOT INTERVALS",Npts
760    REM
770    REM   Eint is defined as the integration or plot interval
780    REM
790         Eint=(Ephotonmax-Ephoton(1))/(Npts-1)
800         Sum=0
810         Sump=0
820         Sumn=0
830    REM
840    REM
850    REM
860    FOR I=1 TO Npts
870         Ephoton=Ephoton(1)+(I-1)*Eint
880                   Ephoton(I)=Ephoton
890         Sigmanu=Sigmam/(1+(Ephoton^2-Egdr^2)^2/(Ephoton^2*Width^2))
900                   Sigmanu(I)=Sigmanu
910         Ecutoff=Hbarc*Gamma*Vel/Bmin
920         G=Ephoton/Ecutoff
930         CALL Bessel(G,K0,K1)
940         Ne=2*Zt^2*Fsc/(Ephoton*PI*Vel^2)*(G*K0*K1-.5*Vel^2*G^2*(K1^2-K0^2))
950                   Ne(I)=Ne
960          Function=Sigmanu*Ne
970          IF I=1 THEN Function=.5*Function
980          IF I=Npts THEN Function=.5*Function
990          Sum=Sum+Function
1000            Functionp=Fracproton*Function
1010            Functionn=(1-Fracproton)*Function
1020            IF Ephoton<Ethreshgp THEN Functionp=0
1030            IF Ephoton<Ethreshgn THEN Functionn=0
1040            Sump=Sump+Functionp
1050            Sumn=Sumn+Functionn
1060    NEXT I
1070   REM
1080   REM
1090   REM
1100        Integralp=Eint*Sump
1110        Integraln=Eint*Sumn
1120        Integral=Integralp+Integraln
1130        PRINT
1140   PRINT
1150   PRINT "Width (MeV)",Width
1160   PRINT "Zt",Zt
1170   PRINT "At",At
1180   PRINT "Zp",Zp
1190   PRINT "Ap",Ap
1200   PRINT "KE/N (MeV/N)",Tlab
1210   PRINT "PHOTON ENERGY (MeV)",Ephoton
1220   PRINT
1230   PRINT
1240   PRINT
1250   PRINT "Lower limit of integration (MeV)",Ephoton(1)
```

```
1260    PRINT "Upper limit of integration (MeV)",Ephotonmax
1270    PRINT "Number of integration intervals is",Npts
1280    PRINT "Value of integration interval width (MeV)",Eint
1290    PRINT
1300    PRINT
1310    PRINT "Sigmanu (mb)",Sigmanu
1320    PRINT "Sigmam (mb)",Sigmam
1330    PRINT "Ro (fm)",Ro
1340    PRINT "U",U
1350    PRINT "GDR Energy (MeV)",Egdr
1360    PRINT
1370    PRINT
1380    PRINT
1390    PRINT "PROJ VELOCITY (=Beta factor)-units of c",Vel
1400    PRINT "RELATIVISTIC GAMMA FACTOR OF PROJ (MeV/N)",Gamma
1410    PRINT "Ecutoff  (MeV)",Ecutoff
1420    PRINT "10 percent charge radius of target   (fm)     ",R10t
1430    PRINT "10 percent charge radius of projectile  (fm)",R10p
1440    PRINT "Dee",Dee
1450    PRINT "Bmin  (fm)",Bmin
1460    PRINT "N(E)  (1/MeV)",Ne
1470    PRINT
1480    PRINT
1490    PRINT "Mass excess of projectile  (MeV)",Mexcessp
1500    PRINT "Mass excess of (proj - neutron)  (MeV)",Mexcessgn
1510    PRINT "Mass excess of (proj - proton)   (MeV) ",Mexcessgp
1520    PRINT
1530    PRINT "COULOMB DISSOCIATION CROSS SECTION (Sigmaww)  (mb)",Integral
1540    PRINT
1550    PRINT "Sigma(gamma,p)   (mb)",Integralp
1560    PRINT "Sigma(gamma,n)   (mb)",Integraln
1570    STOP
1580    END
1590      SUB Bessel(G,K0,K1)
1600      A1=3.5156229
1610      A2=3.0899424
1620      A3=1.2067492
1630      A4=.2659732
1640      A5=.0360768
1650      A6=.0045813
1660      A7=.39894228
1670      A8=.01328592
1680      A9=.00225319
1690      A10=.00157565
1700      A11=.00916281
1710      A12=.02057706
1720      A13=.02635537
1730      A14=.01647633
1740      A15=.00392377
1750      A16=.87890594
1760      A17=.51498869
1770      A18=.15084934
1780      A19=.02658733
1790      A20=.00301532
1800      A21=.00032411
1810      A22=.39894228
1820      A23=.03988024
1830      A24=.00362018
1840      A25=.00163801
1850      A26=.01031555
1860      A27=.02282967
1870      A28=.02895312
1880      A29=.01787654
1890      A30=.00420059
1900      B1=.57721566
1910      B2=.42278420
```

```
1920       B3=.23069756
1930       B4=.0348859
1940       B5=.00262698
1950       B6=.0001075
1960       B7=.0000074
1970       B8=1.25331414
1980       B9=.07832358
1990       B10=.02189568
2000       B11=.01062446
2010       B12=.00587872
2020       B13=.00251540
2030       B14=.00053208
2040       B15=.15443144
2050       B16=.67278579
2060       B17=.18156897
2070       B18=.01919402
2080       B19=.00110404
2090       B20=.00004686
2100       B21=1.25331414
2110       B22=.23498619
2120       B23=.03655620
2130       B24=.01504268
2140       B25=.00780353
2150       B26=.00325614
2160       B27=.00068245
2170   T=G/3.75
2180   IF G<=3.75 THEN I0=1+A1*T^2+A2*T^4+A3*T^6+A4*T^8+A5*T^10+A6*T^12
2190   IF G>3.75 THEN I0=1/SQR(G)*EXP(G)*(A7+A8/T+A9/T^2-A10/T^3+A11/T^4-A12/T^5+
A13/T^6-A14/T^7+A15/T^8)
2200   IF G<=3.75 THEN I1=G*(.5+A16*T^2+A17*T^4+A18*T^6+A19*T^8+A20*T^10+A21*T^12
)
2210   IF G>3.75 THEN I1=1/SQR(G)*EXP(G)*(A22-A23/T-A24/T^2+A25/T^3-A26/T^4+A27/T
^5-A28/T^6+A29/T^7-A30/T^8)
2220   S=G/2
2230   IF G<=2 THEN K0=-LOG(S)*I0-B1+B2*S^2+B3*S^4+B4*S^6+B5*S^8+B6*S^10+B7*S^12
2240   IF G>2 THEN K0=1/SQR(G)*EXP(-G)*(B8-B9/S+B10/S^2-B11/S^3+B12/S^4-B13/S^5+B
14/S^6)
2250   IF G<=2 THEN K1=LOG(S)*I1+1/G*(1+B15*S^2-B16*S^4-B17*S^6-B18*S^8-B19*S^10-
B20*S^12)
2260   IF G>2 THEN K1=1/SQR(G)*EXP(-G)*(B21+B22/S-B23/S^2+B24/S^3-B25/S^4+B26/S^5
-B27/S^6)
2270   SUBEND
```

Note: The large array of numbers listed in the subroutine are parameters for
determining the Bessel functions as given in reference 37.

```
Width (MeV)              5.00
Zt                      82.00
At                     208.00
Zp                      26.00
Ap                      56.00
KE/N (MeV/N)          1880.00
PHOTON ENERGY (MeV)     50.00



Lower limit of integration (MeV)        9.67
Upper limit of integration (MeV)       50.00
Number of integration intervals is    100.00
Value of integration interval width (MeV)            .41



Sigmanu (mb)            1.40
Sigmam (mb)           106.41
Ro (fm)                 4.51
U                       1.70
GDR Energy (MeV)       18.40



PROJ VELOCITY (=Beta factor)-units of c   .94
RELATIVISTIC GAMMA FACTOR OF PROJ (MeV/N)            3.00
Ecutoff (MeV)          42.61
10 percent charge radius of target    (fm)          7.63
10 percent charge radius of projectile  (fm)        5.28
Dee                     0.00
Bmin  (fm)             13.11
N(E)  (1/MeV)            .08



Mass excess of projectile  (MeV)        -60.60
Mass excess of (proj - neutron)  (MeV)  -57.48
Mass excess of (proj - proton)   (MeV)  -57.71

COULOMB DISSOCIATION CROSS SECTION (Sigmaww)  (mb)      902.37

Sigma(gamma,p)  (mb)                 253.37
Sigma(gamma,n)  (mb)                 644.00
```

A	nucleon number
A_p	nucleon number of projectile
A_t	nucleon number of target
BRE	branching ratio equations
b_{min}	minimum impact parameter, fm
C	half-density radius, fm
c	speed of light, 3×10^8 m/sec
d	overlap distance, fm
E	energy, MeV
$E_o(X)$	threshold energy, MeV
E_{GDR}	giant dipole resonance energy, MeV
e	electronic charge, 1.6×10^{-19} coul
GDR	giant dipole resonance
g_n	neutron branching ratio
g_p	proton branching ratio
g_X	branching ratio
$\hbar$	Planck's constant, 6.58×10^{-22} MeV-sec
I	intensity
J	nuclear liquid drop parameter, 36.8 MeV
K_0, K_1	modified Bessel functions of second kind
M	mass, MeV/c^2
m*	7/10 nucleon mass, 657 MeV/c^2
N(E)	virtual photon number spectrum, MeV^{-1}
N_p	neutron number of projectile
N_t	neutron number of target
n	neutron
P	projectile

18

P'	prefragment
p	proton
Q	Q-value, MeV
Q'	nuclear liquid drop parameter, 17 MeV
q	momentum transfer
R_o	nuclear radius, $r_o A^{1/3}$, fm
$R_{0.1}$	10-percent-charge density radius, fm
r	distance, fm
r_o	radius parameter, 1.18 fm
T	target
T'	excited target
T_{th}	threshold energy, MeV
u	nuclear liquid drop parameter
v	speed
w	nuclear density parameter
X	abladed particles
x	energy parameter
Z	proton number
Z_p	proton number of projectile
Z_t	proton number of target
z	diffuseness, fm
α	electromagnetic fine structure constant, 1/137
β	velocity in units of c
Γ	GDR width, MeV
γ	relativistic factor
ε	nuclear liquid drop parameter, 0.0768
$\rho(r)$	nuclear density, fm^{-3}
ρ_o	nuclear central density, fm^{-3}

σ	cross section, mb
σ_{abs}	absorption cross section, mb
σ_{EM}	electromagnetic dissociation cross section, mb
σ_{EM-abs}	electromagnetic absorption cross section, mb
σ_m	cross section parameter, mb
σ_{TRK}	Thomas-Reiche-Kuhn cross section, mb
σ_ν	photonuclear cross section, mb

REFERENCES

1. Haffner, James W.: Radiation and Shielding in Space. Academic Press, Inc., 1967.

2. Todd, Paul: Unique Biological Aspects of Radiation Hazards - An Overview. Adv. Space Res., vol. 3, no. 8, 1983, pp. 187-194.

3. Fry, R. J. M.; Powers-Risius, P.; Alpen, E. L.; Ainsworth, E. J.; and Ullrich, R. L.: High-LET Radiation Carcinogenesis. Adv. Space Res., vol. 3, no. 8, 1983, pp. 241-248.

4. Bergtold, D. S.; Cox, A. B.; Su, C. M.; and Lett, J. T.: Late Skin Damage in Rabbits and Monkeys After Exposure to Particulate Radiations. Adv. Space Res., vol. 3, no. 8, 1983, pp. 221-229.

5. Wilson, John W.: Composite Particle Reaction Theory. Ph.D. Diss., College of William and Mary in Virginia, June 1975.

6. Wilson, J. W.: Multiple Scattering of Heavy Ions, Glauber Theory, and Optical Model. Phys. Lett., vol. B52, no. 2, Sept. 1974, pp. 149-152.

7. Wilson, John W.; and Costner, Christopher M.: Nucleon and Heavy-Ion Total and Absorption Cross Section for Selected Nuclei. NASA TN D-8107, 1975.

8. Wilson, J. W.; and Townsend, L. W.: An Optical Model for Composite Nuclear Scattering. Canadian J. Phys., vol. 59, no. 11, Nov. 1981, pp. 1569-1576.

9. Townsend, Lawrence W.: Optical-Model Abrasion Cross Sections for High-Energy Heavy Ions. NASA TP-1893, 1981.

10. Townsend, L. W.; and Wilson, J. W.: Comment on "Nucleus-Nucleus Total Reaction Cross Sections." Phys. Rev., ser. C, vol. 25, no. 3, Mar. 1982, pp. 1679-1681.

11. Townsend, Lawrence W.: Harmonic Well Matter Densities and Pauli Correlation Effects in Heavy-Ion Collisions. NASA TP-2003, 1982.

12. Townsend, L. W.; Wilson, J. W.; and Bidasaria, H. B.: On the Geometric Nature of High-Energy Nucleus-Nucleus Reaction Cross Sections. Canadian J. Phys., vol. 60, no. 10, Oct. 1982, pp. 1514-1518.

13. Townsend, Lawrence W.; Wilson, John W.; and Bidasaria, Hari B.: Heavy-Ion Total and Absorption Cross Sections Above 25 MeV/Nucleon. NASA TP-2138, 1983.

14. Townsend, Lawrence W.; Wilson, John W.; and Bidasaria, Hari B.: Nucleon and Deuteron Scattering Cross Sections From 25 MeV/Nucleon to 22.5 GeV/Nucleon. NASA TM-84636, 1983.

15. Townsend, L. W.: Abrasion Cross Sections for ^{20}Ne Projectiles at 2.1 GeV/Nucleon. Canadian J. Phys., vol. 61, no. 1, Jan. 1983, pp. 93-98.

16. Townsend, Lawrence W.; Wilson, John W.; Norbury, John W.; and Bidasaria, Hari B.: An Abrasion-Ablation Model Description of Galactic Heavy-Ion Fragmentation. NASA TP-2305, 1984.

17. Norbury, John W.; Townsend, Lawrence W.; and Deutchman, Philip A.: A T-Matrix Theory of Galactic Heavy-Ion Fragmentation. NASA TP-2363, 1985.

18. Wilson, John W.; and Lampkin, Stanley L.: Perturbation Theory for Charged-Particle Transport in One Dimension. Nucl. Sci. & Eng., vol. 57, no. 4, Aug. 1975, pp. 292-299.

19. Wilson, John W.: Analysis of the Theory of High-Energy Ion Transport. NASA TN D-8381, 1977.

20. Wilson, John W.: Heavy Ion Transport in the Straight Ahead Approximation. NASA TP-2178, 1983.

21. Wilson, John W.; Townsend, L. W.; Bidasaria, H. B.; Schimmerling, Walter; Wong, Mervyn; and Howard, Jerry: ^{20}Ne Depth-Dose Relations in Water. Health Phys., vol. 46, no. 5, May 1984, pp. 1101-1111.

22. Pilkuhn, H.: Dissociation of Relativistic Nuclei in the Nuclear Coulomb Field. Phys. Lett., ser. B, vol. 38, no. 3, Feb. 7, 1972, pp. 143-146.

23. Artru, X.; and Yodh, G. B.: Coulomb Dissociation of Relativistic Nuclei. Phys. Lett., ser. B, vol. 40, no. 1, June 12, 1972, pp. 43-45.

24. Faldt, G.; Pilkuhn, H.; and Schlaile, H. G.: Nucleus-Nucleus Collisions at Relativistic Energies. Ann. Phys., vol. 82, no. 2, Feb. 1974, pp. 326-344.

25. Jäckle, R.; and Pilkuhn, H.: Profile Functions for Coulomb Excitation at High Energies. Nucl. Phys., ser. A, vol. 247, no. 3, Aug. 11, 1975, pp. 521-528.

26. Heckman, Harry H.; and Lindstrom, Peter J.: Coulomb Dissociation of Relativistic ^{12}C and ^{16}O Nuclei. Phys. Rev. Lett., vol. 37, no. 1, July 5, 1976, pp. 56-59.

27. Westfall, G. D.; Wilson, Lance W.; Lindstrom, P. J.; Crawford, H. J.; Greiner, D. E.; and Heckman, H. H.: Fragmentation of Relativistic ^{56}Fe. Phys. Rev., ser. C, vol. 19, no. 4, Apr. 1979, pp. 1309-1323.

28. Olson, D. L.; Berman, B. L.; Greiner, D. E.; Heckman, H. H.; Lindstrom, P. J.; Westfall, G. D.; and Crawford, H. J.: Electromagnetic Dissociation of Relativistic ^{18}O Nuclei. Phys. Rev., ser. C, vol. 24, no. 4, Oct. 1981, pp. 1529-1539.

29. Mercier, M. T.; Hill, J. C.; Wohn, F. K.; and Smith, A. R.: Electromagnetic Dissociation of ^{197}Au by Relativistic Heavy Ions. Phys. Rev. Lett., vol. 52, no. 11, Mar. 12, 1984, pp. 898-901.

30. Goldberg, A.: On the Virtual Photon Spectrum for Electromagnetic Dissociation of Relativistic Nuclei in Peripheral Collisions. Nucl. Phys., ser. A, vol. 420, no. 3, June 4, 1984, pp. 636-644.

31. Gross, Franz; and Whitney, R. Roy, eds.: Proceedings CEBAF/SURA 1984 Summer Workshop. Continuous Electron Beam Accelerator Facility, Nov. 1984.

32. Williams, E. J.: Correlation of Certain Collision Problems With Radiation Theory. Kgl. Danske Videnskab. Selskab Math.-Fys. Medd., vol. XIII, no. 4, 1935.

33. Heitler, W.: The Quantum Theory of Radiation, Third ed. Clarendon Press (Oxford), 1954, appendix 6.

34. Panofsky, Wolfgang K. H.; and Phillips, Melba: Classical Electricity and Magnetism, Second ed., Addison-Wesley Pub. Co., Inc., c.1962, sec. 18.5.

35. Jackson, John David: Classical Electrodynamics, Second ed., John Wiley & Sons, Inc., c.1975, ch. 15.

36. Spiegel, Murray R.: Mathematical Handbook of Formulas and Tables. McGraw-Hill Book Co., c.1968.

37. Abramowitz, Milton; and Stegun, Irene A., eds.: Handbook of Mathematical Functions With Formulas, Graphs, and Mathematical Tables. NBS Appl. Math. ser. 55, U.S. Dep. Commerce, June 1964.

38. Spicer, B. M.: The Giant Dipole Resonance. Advances in Nuclear Physics, Volume 2, Michel Baranger and Erich Vogt, eds., Plenum Press, Inc., 1969, pp. 1-78.

39. Berman, B. L.; and Fultz, S. C.: Measurements of the Giant Dipole Resonance With Monoenergetic Photons. Rev. Mod. Phys., vol. 47, no. 3, July 1975, pp. 713-761.

40. Norbury, John William: Isobaric Spin Splitting and Deformation Effects of the Giant Dipole Resonance in ^{54}Fe and the Photodeuteron Yield From ^{32}S. 4th Year Report, Univ. of Melbourne, 1976.

41. Norbury, John William: The ^{54}Fe(γ,n) and ^{32}S(γ,d) Cross Sections. M.S. Thesis, Univ. of Melbourne, Nov. 1978.

42. Norbury, J. W.; Thompson, M. N.; Shoda, K.; and Tsubota, H.: Photoneutron Cross Section of ^{54}Fe. Australian J. Phys., vol. 31, no. 6, Dec. 1978, pp. 471-475.

43. Levinger, Joseph S.: Nuclear Photo-Disintegration. Oxford Univ. Press, 1960.

44. Weinstock, E. V.; and Halpern, J.: Systematics of Photoproton Reactions. Phys. Rev., vol. 94, no. 6, June 15, 1954, pp. 1651-1654.

45. Woodworth, J. G.; McNeill, K. G.; Jury, J. W.; Alvarez, R. A.; Berman, B. L.; Faul, D. D.; and Meyer, P.: Photonuclear Cross Sections for ^{18}O. Phys. Rev., ser. C, vol. 19, no. 5, May 1979, pp. 1667-1683.

46. De Jager, C. W.; De Vries, H.; and De Vries, C.: Nuclear Charge- and Magnetization-Density-Distribution Parameters From Elastic Electron Scattering. At. Data & Nucl. Data Tables, vol. 14, no. 5/6, Nov./Dec. 1974, pp. 479-508.

TABLE 1.- RESONANCE WIDTHS AND PARTICLE BRANCHING RATIOS

[Numbers to left of column have been confronted with experiment, numbers to right are our estimates used in present calculations]

Nucleus	Γ, MeV		g_p		g_n	
^{7}Li						
^{9}Be						
^{12}C	[a]8.0			[b]0.5	[b]0.5	
^{16}O	[a]10.0			[b]0.5	[b]0.5	
^{18}O	[a]12.0		[a]0.4		[a]0.6	
^{20}Ne		[c]10.0		[b]0.5		[b]0.5
^{28}Si	[a]10.0			[b]0.5	[b]0.5	
^{32}S						
^{40}Ar		[c]10.0		[b]0.45		[b]0.55
^{40}Ca		[c]10.0		[b]0.5		[b]0.5
^{48}Ti						
^{54}Fe	[a]3.0		[a]0.7		[a]0.3	
^{56}Fe		[c]5.0		[b]0.28		[b]0.72
^{58}Ni	[a]10.0			[b]0.5	[b]0.5	
^{63}Cu		[c]5.0		[b]0.28		[b]0.72
^{90}Zr	[d]4.0			[b]0.05	[b]0.95	
^{107}Ag		[c]5.0		[b]0		[b]1.0
^{160}Gd	[d]4.0			[b]0	[b]1.0	
^{181}Ta						
^{197}Au	[a,d]3.5			[b]0	[b]1.0	
^{208}Pb	[d]3.9			[b]0	[b]1.0	
^{238}U	[a]5.0			[b]0	[b]1.0	

[a]Fitted to data.
[b]Obtained from the BRE.
[c]Estimate.
[d]Taken from Berman and Fultz (ref. 39).

TABLE 2.- GIANT DIPOLE RESONANCE ENERGIES AND PARTICLE THRESHOLDS

$$\left[\begin{array}{c}\text{Energies were calculated by equation (1); thresholds calculated} \\ \text{by equation (A2)}\end{array}\right]$$

Nucleus	GDR energy, MeV	Proton threshold, MeV	Neutron threshold, MeV
^{12}C	25.6	15.46	18.74
^{16}O	24.1	11.62	15.67
^{18}O	23.5	15.44	8.05
^{40}Ar	19.8	12.02	9.87
^{56}Fe	18.4	9.67	11.20
^{197}Au	13.7	5.27	8.07

TABLE 3.- THE 10-PERCENT-CHARGE DENSITY RADII

Nucleus	10-percent radius, fm	Model (a)
^{7}Li	3.04	HO
^{9}Be	3.32	HO
^{12}C	3.33	HO
^{16}O	3.77	HO and 3pF
^{18}O	3.88	HO
^{20}Ne	4.06	2pF
^{27}Al	4.21	2pF
^{28}Si	4.18	2pF
^{32}S	4.53	3pF
^{40}Ar	4.73	2pF and 3pF
^{40}Ca	4.80	2pF and 3pF
^{48}Ti	5.00	2pF
^{54}Fe	5.19	2pF
^{56}Fe	5.28	2pF
^{58}Ni	5.37	2pF
^{64}Cu	5.45	2pF
^{90}Zr	5.90	3pG
^{108}Ag and ^{107}Ag	6.32	2pF
^{160}Gd		
^{181}Ta	7.79	2pF
^{197}Au	7.56	2pF
^{208}Pb	7.83	2pF and 3pG
^{238}U	8.13	2pF

[a]The models are defined in appendix B and are as follows: HO, harmonic-oscillator; 2pF, 2-parameter Fermi; 3pF, 3-parameter Fermi; and 3pG, 3-parameter Gaussian.

TABLE 4.- CALCULATED TOTAL ELECTROMAGNETIC ABSORPTION CROSS SECTION FOR 1.88 GeV/N ^{56}Fe INCIDENT UPON VARIOUS TARGETS

Projectile	Energy, GeV/N	Target	$\sigma_{EM}(W)$, mb (a)	σ_{EM}, mb, for -	
				d = -1.5 fm	d = 0 fm
^{56}Fe	1.88	$^{7}_{3}$Li	2	1.6	1.9
		$^{9}_{4}$Be	3	2.8	3.3
		$^{12}_{6}$C	7	6.3	7.3
		$^{32}_{16}$S	46	40	46
		$^{63}_{29}$Cu	130	122	140
		$^{107}_{47}$Ag	306		
		$^{181}_{73}$Ta	629	630	717
		$^{208}_{82}$Pb	834	793	901
		$^{238}_{92}$U	1008	973	1105

[a]This column represents the isotope-averaged calculations of Westfall et al. (ref. 27).

TABLE 5.- CALCULATED TOTAL ELECTROMAGNETIC REACTION CROSS SECTIONS FOR ^{12}C AND ^{16}O INCIDENT UPON VARIOUS TARGETS

Projectile	Energy, GeV/N	Target	Final state	σ_{EM}(HL), mb (a)	σ_{EM}, mb, for —	
					d = -1.5 fm	d = 0 fm
^{12}C	2.1	^{208}Pb	^{11}C + n	50 ± 18	46	54
			^{11}B + p	50 ± 25	51	60
	1.05		^{11}C + n	38 ± 24	25	32
			^{11}B + p	50 ± 26	28	36
^{16}O	2.1		^{15}O + n	50 ± 25	67	78
			^{15}N + p	97 ± 17	75	87
^{12}C	2.1	^{108}Ag	^{11}C + n	22 ± 12	18	21
			^{11}B + p	20 ± 12	20	23
	1.05		^{11}C + n	22 ± 12	10.4	13
			^{11}B + p	25 ± 20	11.7	15
^{16}O	2.1		^{15}O + n	26 ± 13	26	30
			^{15}N + p	29 ± 18	29	33
^{12}C	2.1	^{64}Cu	^{11}C + n	10 ± 6	7.5	9
			^{11}B + p	4 ± 8	8.2	10
	1.05		^{11}C + n	10 ± 7	4.5	5.9
			^{11}B + p	5 ± 8	5.1	6.5
^{16}O	2.1		^{15}O + n	10 ± 7	11	12.7
			^{15}N + p	14 ± 9	12	14
^{12}C	2.1	^{27}Al	^{11}C + n	0 ± 3	1.7	2.1
			^{11}B + p	0 ± 3	1.9	2.3
	1.05		^{11}C + n	1 ± 3	1.1	1.5
			^{11}B + p	1 ± 3	1.3	1.6
^{16}O	2.1		^{15}O + n	0 ± 3	2.5	2.9
			^{15}N + p	0 ± 0	2.7	3.2
^{12}C	2.1	^{12}C	^{11}C + n	0 ± 1	0.4	0.50
			^{11}B + p	0 ± 3	0.5	0.54
	1.05		^{11}C + n	0 ± 2	0.3	0.36
			^{11}B + p	0 ± 1	0.3	0.40
^{16}O	2.1		^{15}O + n	0 ± 2	0.58	0.70
			^{15}N + p	0 ± 3	0.64	0.76

[a]This column represents the measurements (isotope averaged) of Heckman and Lindstrom (ref. 26).

TABLE 6.- CALCULATED TOTAL ELECTROMAGNETIC REACTION CROSS SECTIONS FOR ^{18}O AT 1.7 GeV/N INCIDENT UPON VARIOUS TARGETS

Projectile	Energy, GeV/N	Target	Final state	$\sigma_{EM}(0)$, mb (a)	σ_{EM}, mb, for -					
					d = -1.5 fm and g_p of -			d = 0 fm and g_p of -		
					0.4	0.3	0.2	0.4	0.3	0.2
^{18}O	1.7	^{48}Ti	$^{17}O + n$	8.7 ± 2.7	9	10	12	11	12	14
			$^{17}N + p$	-0.5 ± 1.0	5	4	2	6	4	3
		^{208}Pb	$^{17}O + n$	136 ± 2.9	93	108	123	108	127	144
			$^{17}N + p$	20.2 ± 1.8	48	36	24	57	43	29
		^{238}U	$^{17}O + n$	140.8 ± 4.1	113	131	151	132	154	176
			$^{17}N + p$	25.1 ± 1.6	59	44	30	70	52	35

[a]This column represents the measurements (isotope averaged) of Olson et al. (ref. 28).

TABLE 7.- TARGET FRAGMENTATION - CALCULATED TOTAL ELECTROMAGNETIC REACTION CROSS SECTIONS FOR VARIOUS PROJECTILES INCIDENT UPON ^{197}Au

Projectile	Energy, GeV/N	Target	Final state	$\sigma_{EM}(M)$, mb (a)	σ_{EM}, mb, for -	
					d = -1.5 fm	d = 0 fm
^{12}C	2.1	^{197}Au	$^{196}Au + n$	66 ± 20	33	37
^{20}Ne	2.1			136 ± 21	87	97
^{40}Ar	1.8			420 ± 120	250	278
^{56}Fe	1.7			680 ± 160	488	546

[a]This column represents the data of Mercier et al. (ref. 29).

TABLE 8.- ELECTROMAGNETIC DISSOCIATION CROSS SECTIONS FOR A VARIETY
OF REACTIONS WITH $d = 0$ fm

Projectile	Energy	Γ, MeV	g_p	Target	Final state	σ_{EM}, mb
^{12}C	86 MeV/N	8.0	0.5	^{12}C	$^{11}C + n$ $^{11}B + p$	0.09 0.11
	350 MeV/N			^{107}Ag	$^{11}C + n$ $^{11}B + p$	6 7
	1.05 GeV/N			^{197}Au	$^{11}C + n$ $^{11}B + p$	31 34
	2.1 GeV/N			^{197}Au	$^{11}C + n$ $^{11}B + p$	53 57
^{16}O	2.1 GeV/N	10.0	0.5	^{9}Be	$^{15}O + n$ $^{15}N + p$	0.31 0.34
				^{12}C	$^{15}O + n$ $^{15}N + p$	0.71 0.76
				^{208}Pb	$^{15}O + n$ $^{15}N + p$	80 87
^{40}Ar	213 MeV/N	10.0	0.45	^{12}C	$^{39}Ar + n$ $^{39}Cl + p$	1.2 0.9
^{56}Fe	1.88 GeV/N	5.0	0.28	^{12}C	$^{55}Fe + n$ $^{55}Mn + p$	5.3 2.1
				^{108}Ag	$^{55}Fe + n$ $^{55}Mn + p$	242 97
				^{208}Pb	$^{55}Fe + n$ $^{55}Mn + p$	645 258
^{238}U	900 MeV/N	5.0	0	^{12}C	$^{237}U + n$ $^{237}Pa + p$	33 0
				^{27}Al	$^{237}U + n$ $^{237}Pa + p$	142 0
				^{28}Si	$^{237}U + n$ $^{237}Pa + p$	165 0
				^{64}Cu	$^{237}U + n$ $^{237}Pa + p$	628 0
				^{181}Ta	$^{237}U + n$ $^{237}Pa + p$	3208 0
				^{208}Pb	$^{237}U + n$ $^{237}Pa + p$	4034 0

Figure 1.- Schematic diagram of peripheral fragmentation (involving one-nucleon removal) of ^{56}Fe nucleus by ^{208}Pb target.
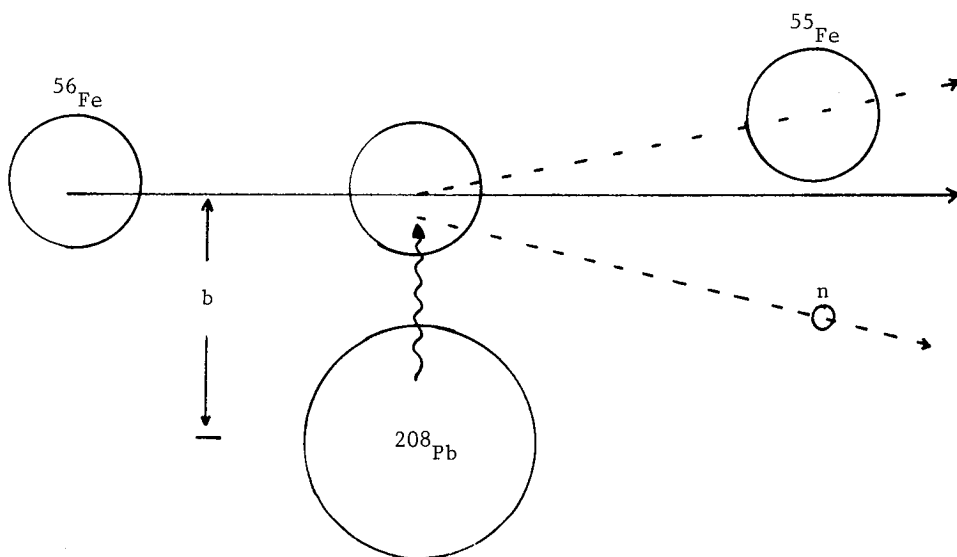
Figure 2.- Schematic diagram of electromagnetic dissociation (involving one-nucleon removal) of ^{56}Fe nucleus by ^{208}Pb target.
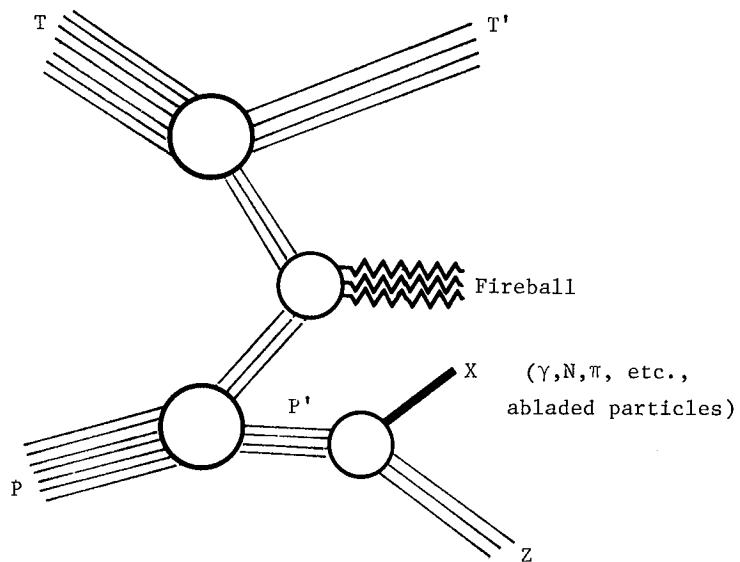
Figure 3.- Reaction diagram of projectile frag-
    mentation induced by nuclear interaction.
    (Final state interactions are ignored.)
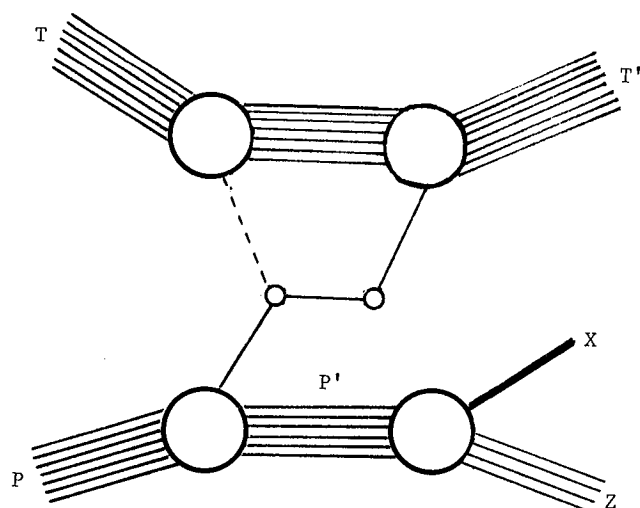
Figure 4.- Reaction diagram of peripheral
    fragmentation involving one-nucleon
    removal.
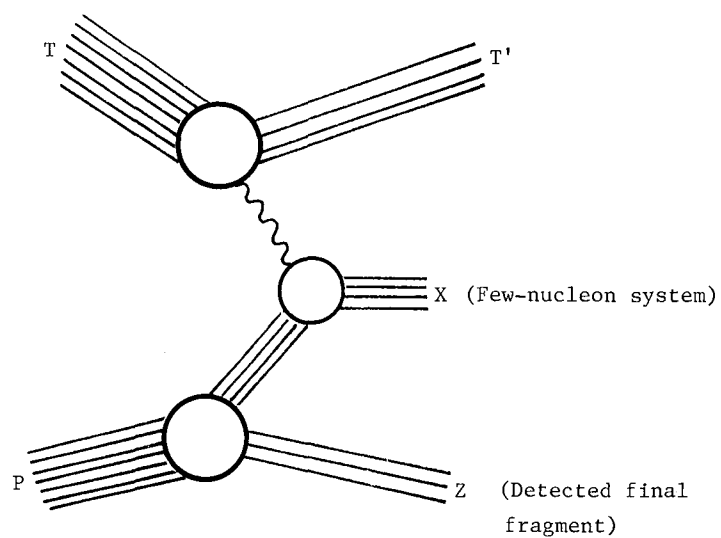
Figure 5.- Reaction diagram of projectile frag-
mentation induced by electromagnetic
interaction.
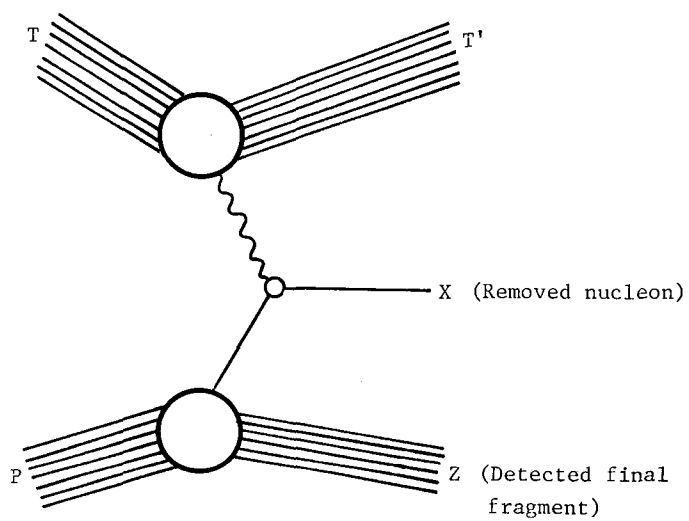
Figure 6.- Reaction diagram of electromag-
netic dissociation leading to one-nucleon
removal.
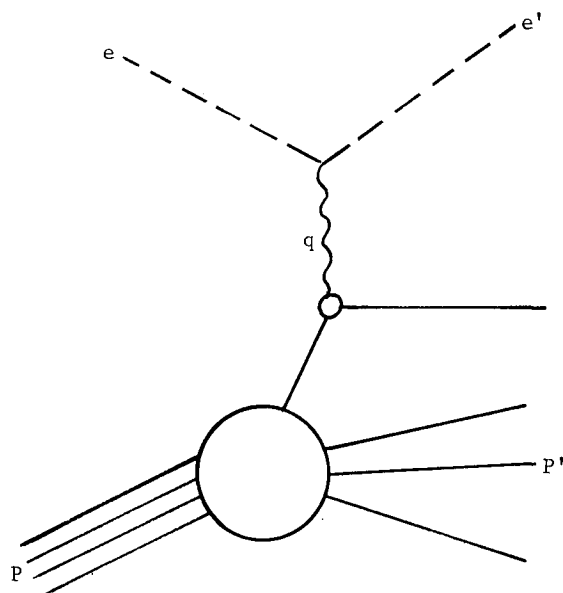
Figure 7.- Reaction diagram of electromagnetic dissociation induced by virtual photon field of an electron such as will be studied at CEBAF.
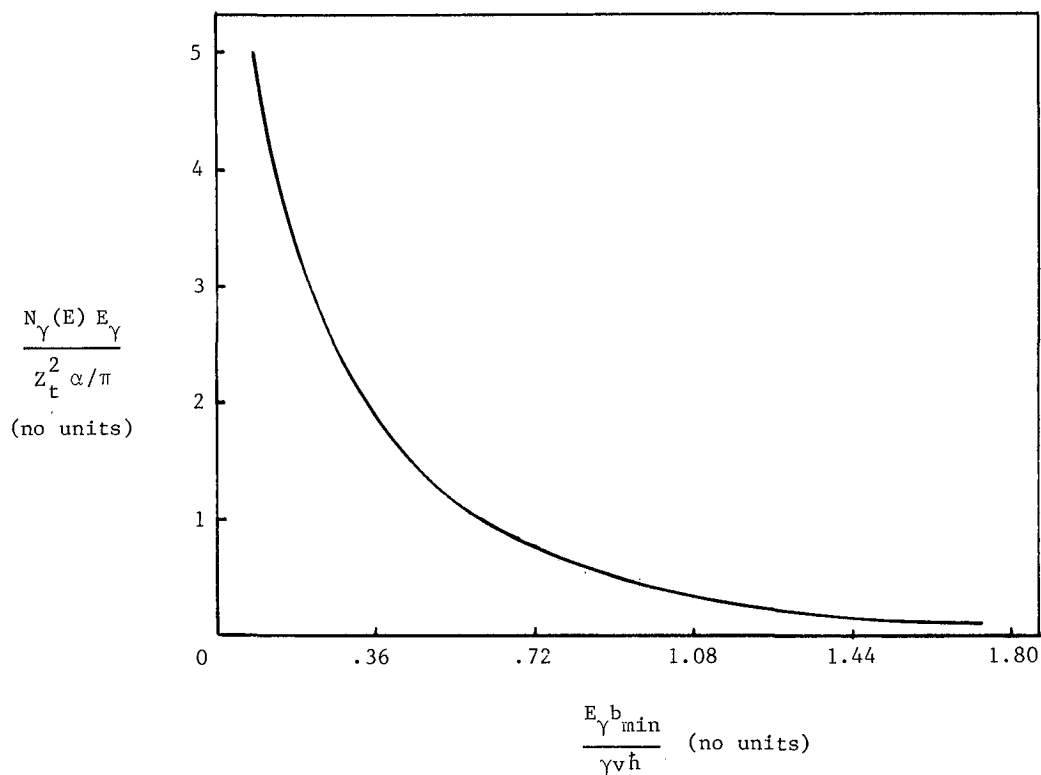
Figure 8.- Frequency spectrum of virtual quanta corresponding to figure 15.8 of Jackson (ref. 35) for the reaction ^{18}O onto ^{238}U at 1.7 GeV/N with the overlap distance $d = -1.5$ fm. The nuclear radii were taken from Olson et al. (ref. 28) and not table 3; thus, $R_{0.1}(^{238}U) = 7.92$ fm, $R_{0.1}(^{18}O) = 3.84$ fm, $b_{min} = 10.2$ fm.
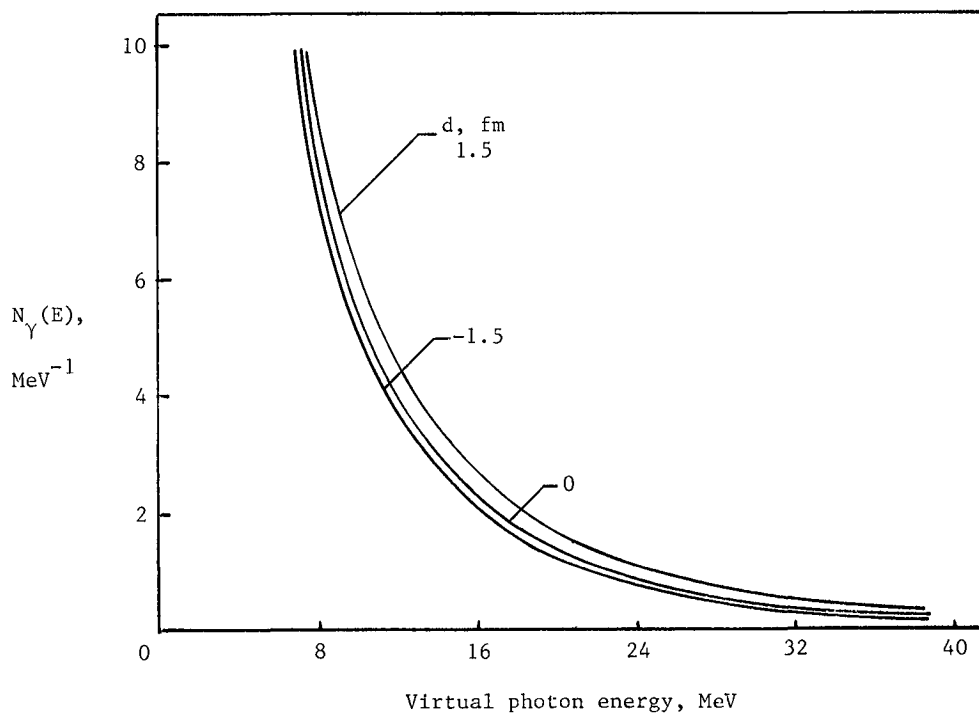
Figure 9.- Number spectrum of virtual quanta as in figure 8.
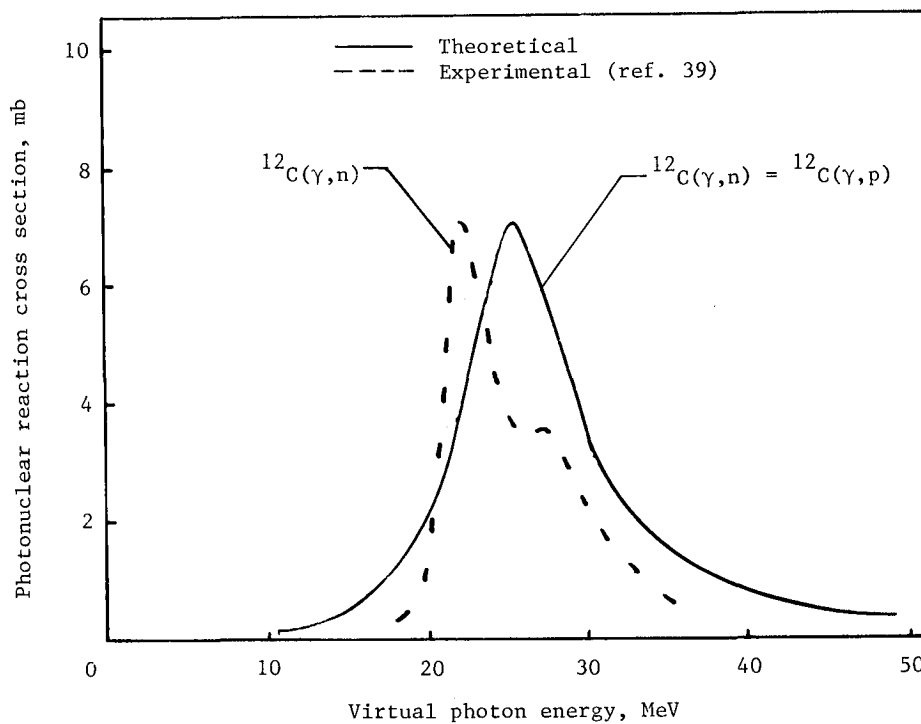
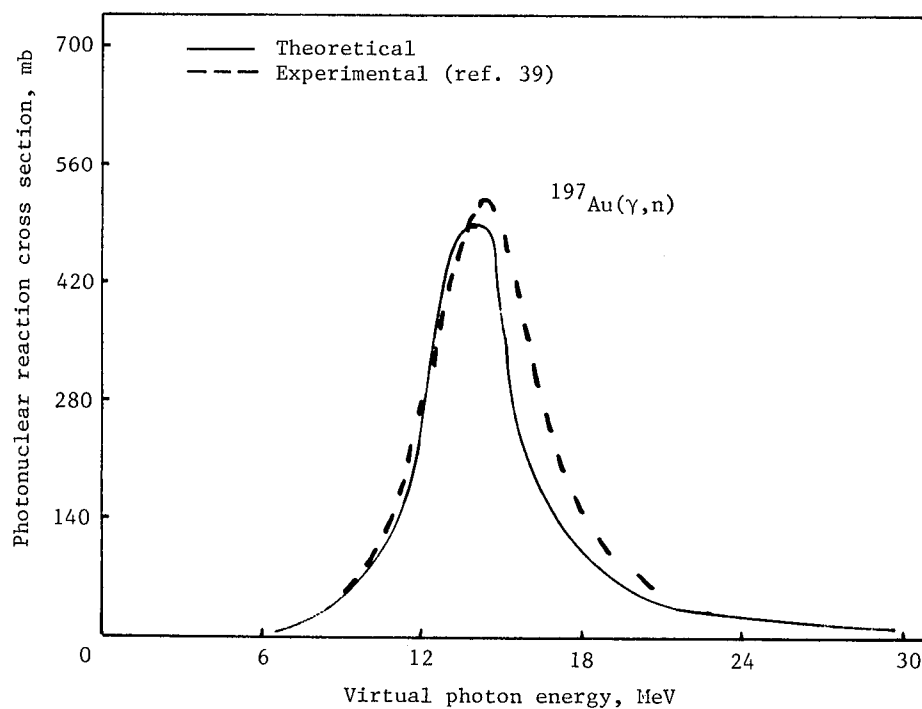
Figure 10.- Theoretical and experimental photoneutron reaction cross section for ^{12}C. Width, $\Gamma = 8$ MeV, has been adjusted to fit data. Proton branching ratio, $g_n = 0.5$, is $1 - Z_p/A_p$; thus, theoretical photoneutron and photoproton cross sections are identical.
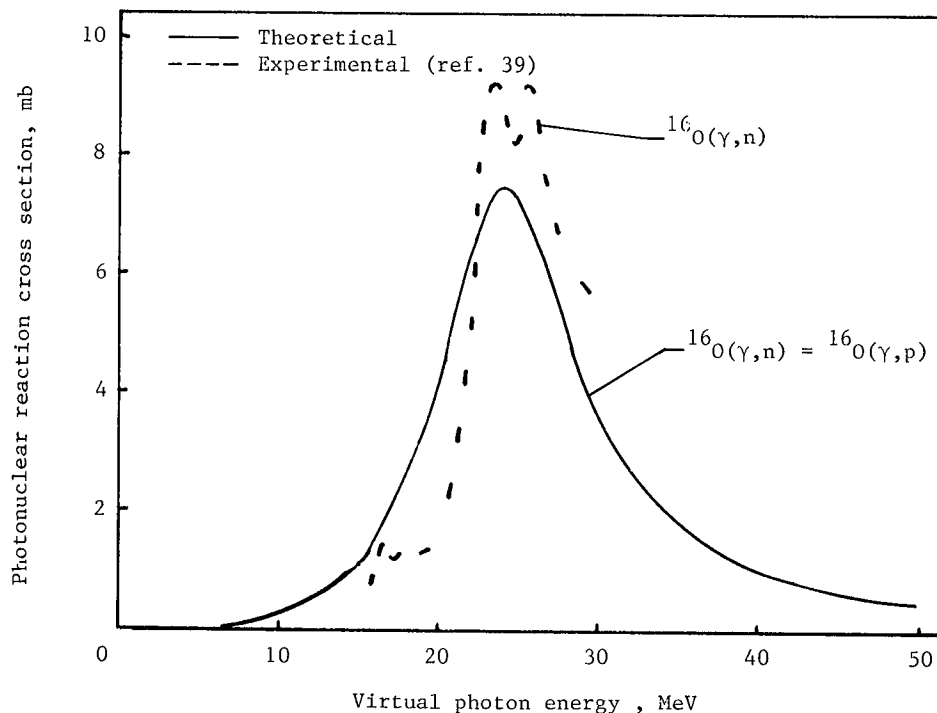
Figure 11.- Theoretical and experimental photoneutron reaction cross section for ^{16}O. Width, Γ = 10 MeV, has been adjusted to fit data. Neutron branching ratio, g_n = 0.5, is $1 - Z_p/A_p$; thus, theoretical photoneutron and photoproton cross sections are identical.
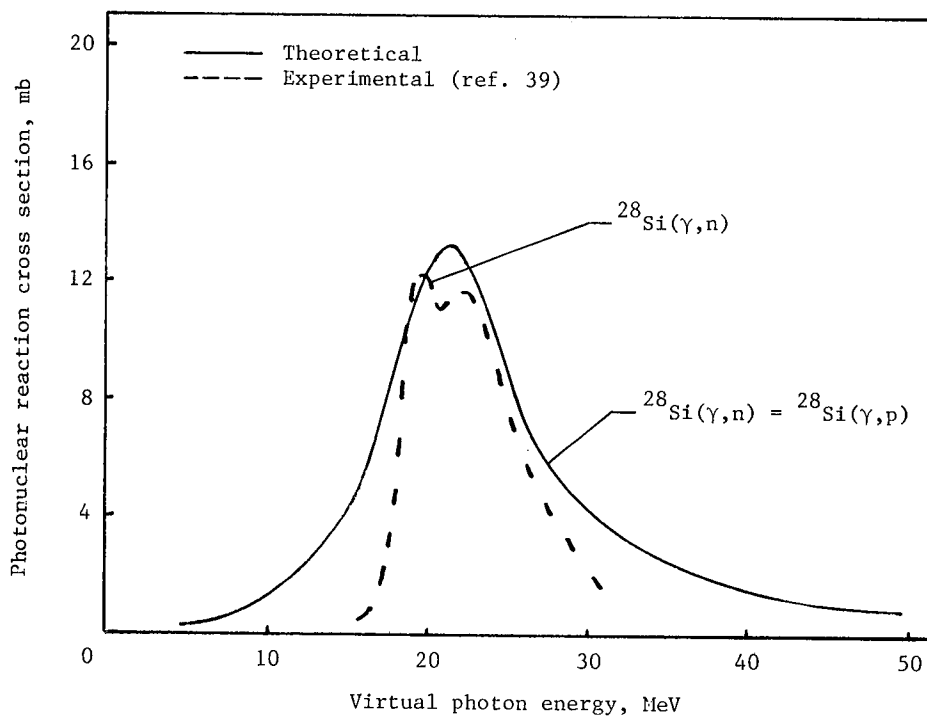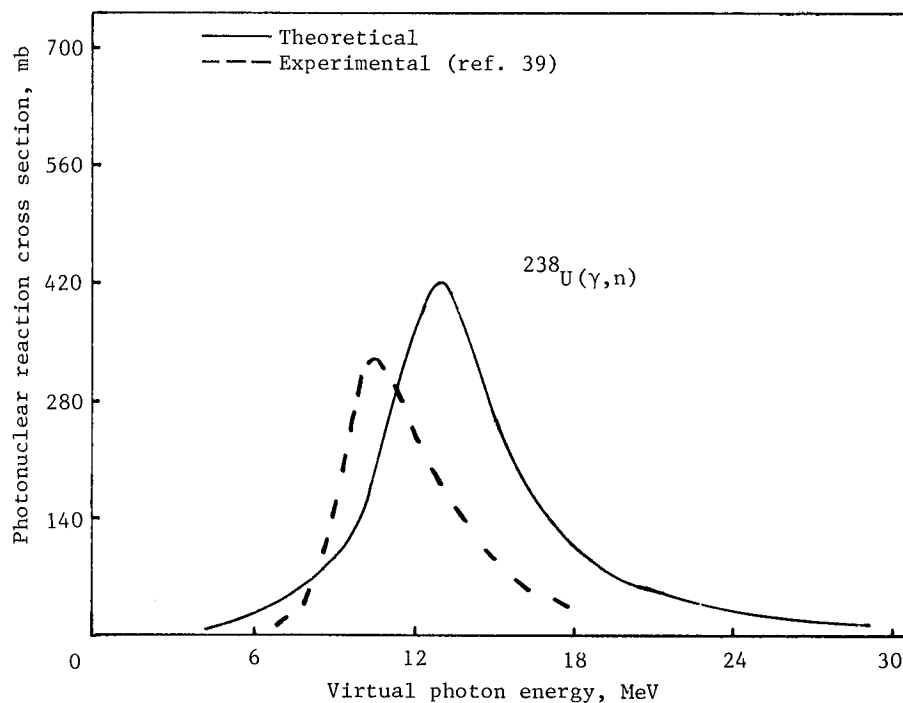

Figure 12.- Theoretical and experimental photoneutron reaction cross section for ^{28}Si. Width, Γ = 10, has been fitted to data. Neutron branching ratio, g_n = 0.5, is $1 - Z_p/A_p$; thus, theoretical photoneutron and photoproton cross sections are identical.
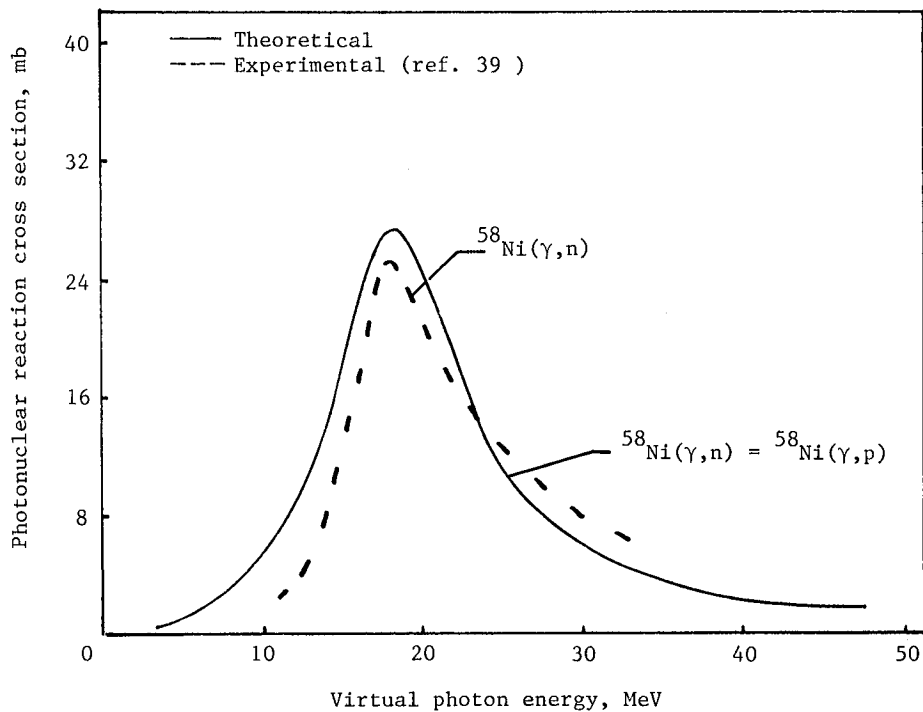
Figure 13.- Theoretical and experimental photoneutron reaction cross section for ^{58}Ni. Width, Γ = 10 MeV, has been fitted to data. Neutron branching ratio, g_n = 0.5, is $1 - Z_p/A_p$; thus, theoretical photoneutron and photoproton cross sections are identical.
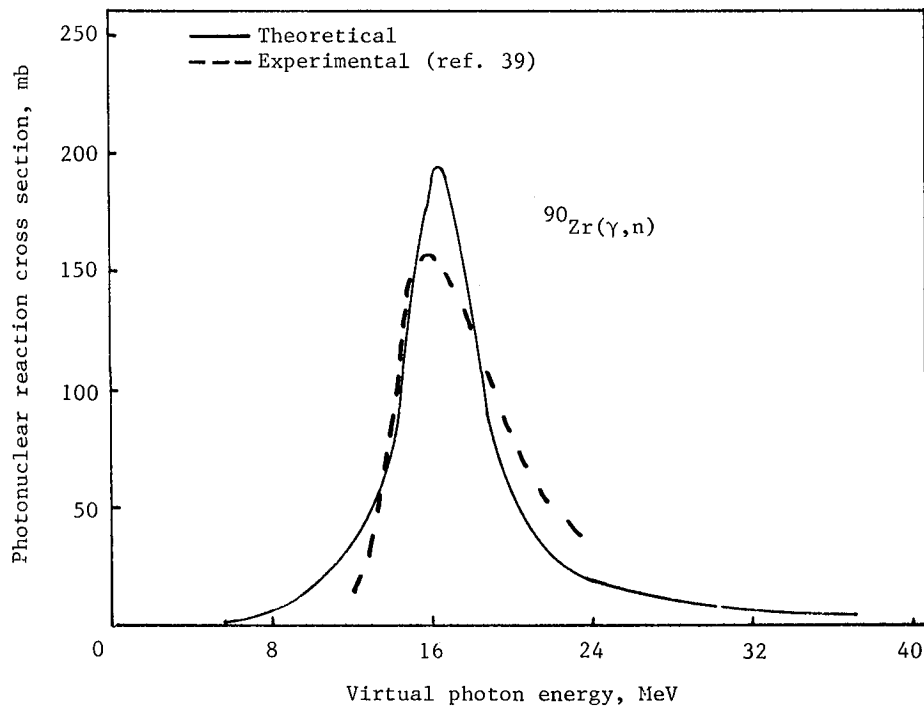
Figure 14.- Theoretical and experimental photoneutron reaction cross section for ^{90}Zr. Width, Γ = 4 MeV, has been obtained from figure 46 of reference 39. Neutron branching ratio, g_n = 0.95, is obtained from proton branching ratio, g_p = 0.05, given in reference 44.

37
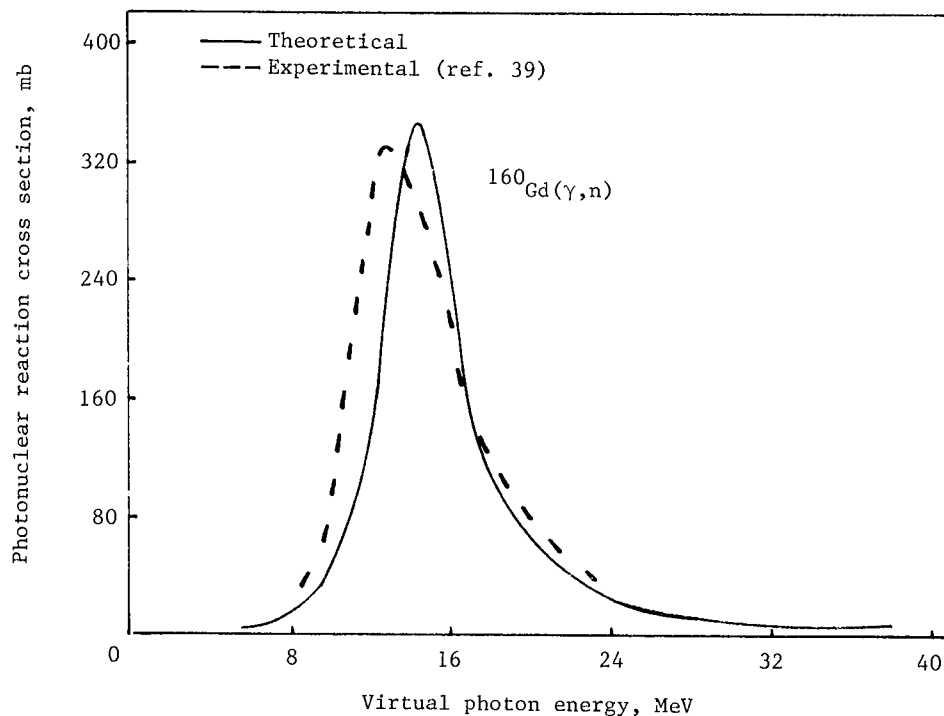
Figure 15.- Theoretical and experimental photoneutron reaction cross section for ^{160}Gd. Width, $\Gamma = 4$ MeV, has been obtained from figure 46 of reference 39. Neutron branching ratio, $g_n \approx 1$, is obtained from proton branching ratio, $g_p \approx 0$, given in reference 44.

Figure 16.- Theoretical and experimental photoneutron reaction cross section for ^{197}Au. Width, $\Gamma = 3.5$, has been obtained by fitting and from figure 46 of reference 39. Neutron branching ratio is $g_n \approx 1$ (ref. 44); thus, photoproton cross section is negligible.
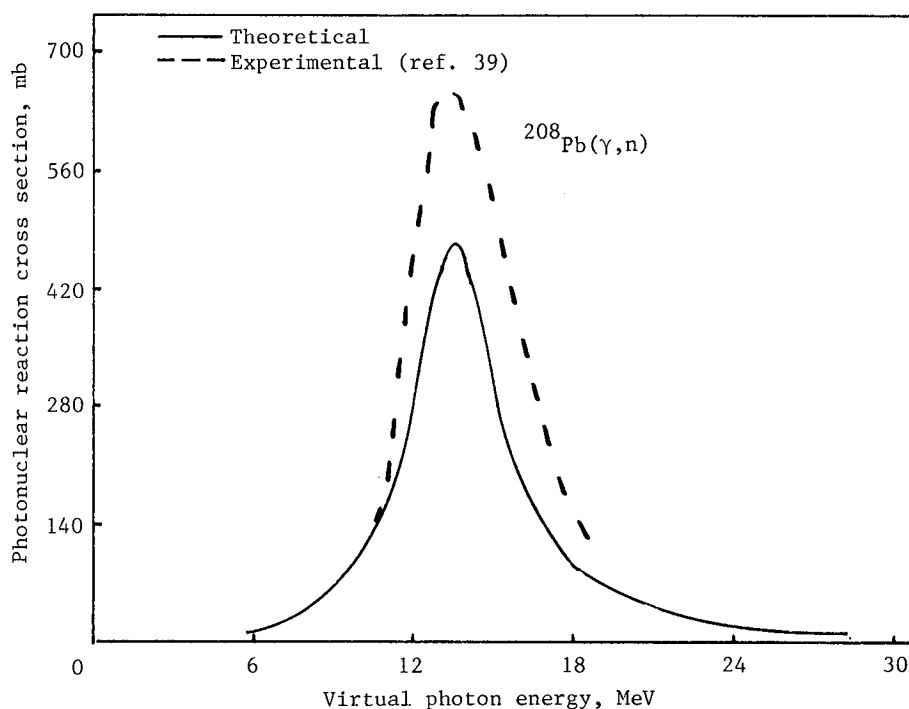
Figure 17.- Theoretical and experimental photoneutron reaction cross section for ^{208}Pb. Width, $\Gamma = 3.9$, has been obtained from figure 46 of reference 39. Neutron branching ratio is $g_n \approx 1$ (ref. 44); thus, photoproton cross section is negligible.

Figure 18.- Theoretical and experimental photoneutron reaction cross section for ^{238}U. Width, $\Gamma = 5$, has been fitted to data. Neutron branching ratio is $g_n \approx 1$ (ref. 44); thus, photoproton cross section is negligible.
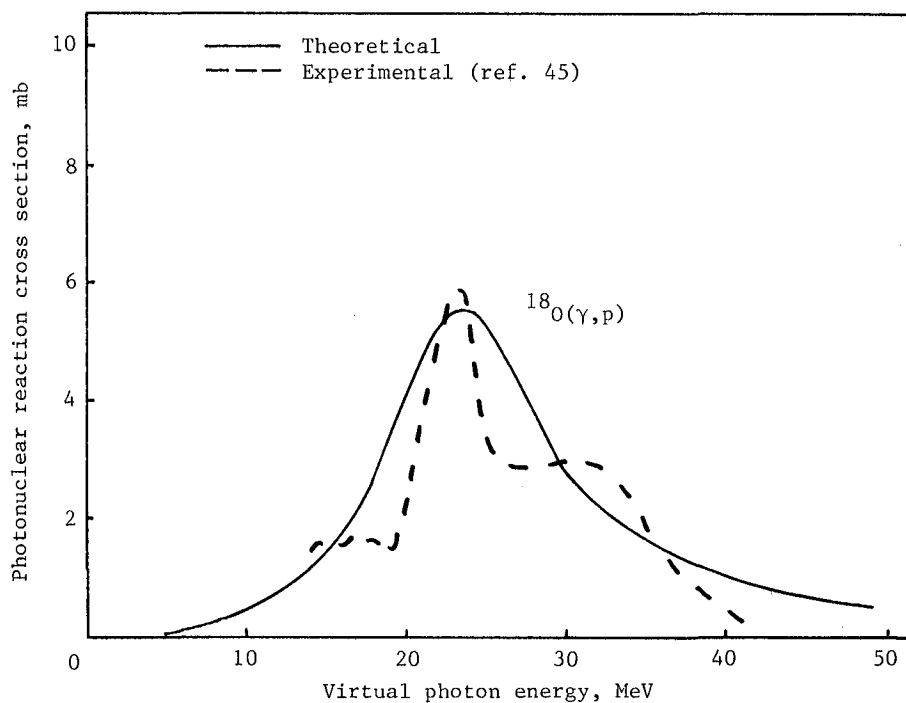
Figure 19.- Theoretical and experimental photoproton reaction cross section for ^{18}O.
Width, Γ = 12 MeV, and proton branching ratio, g_p = 0.4, have both been adjusted
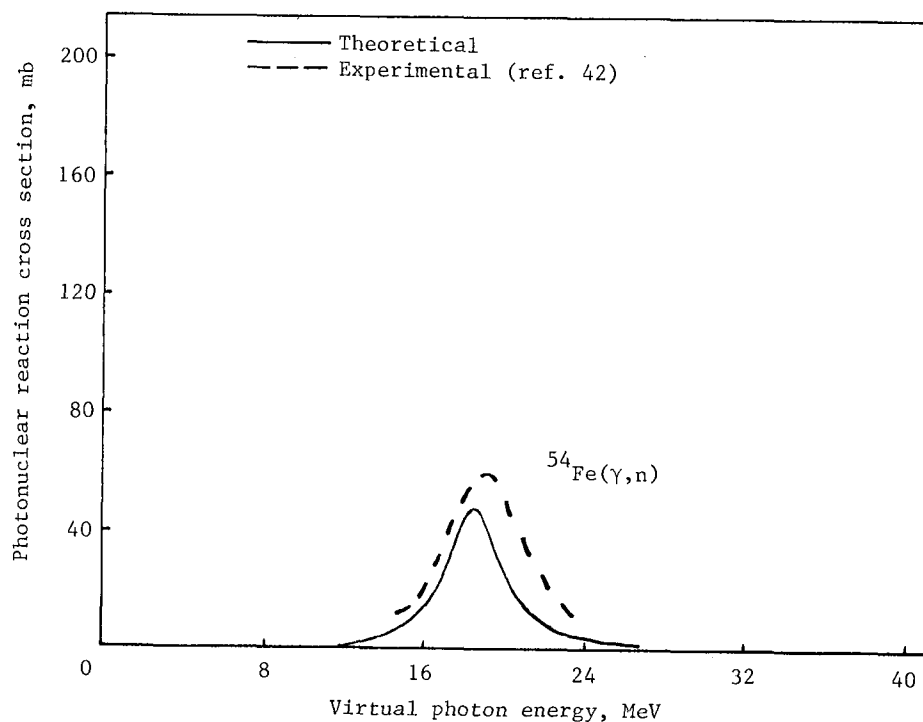to fit data.
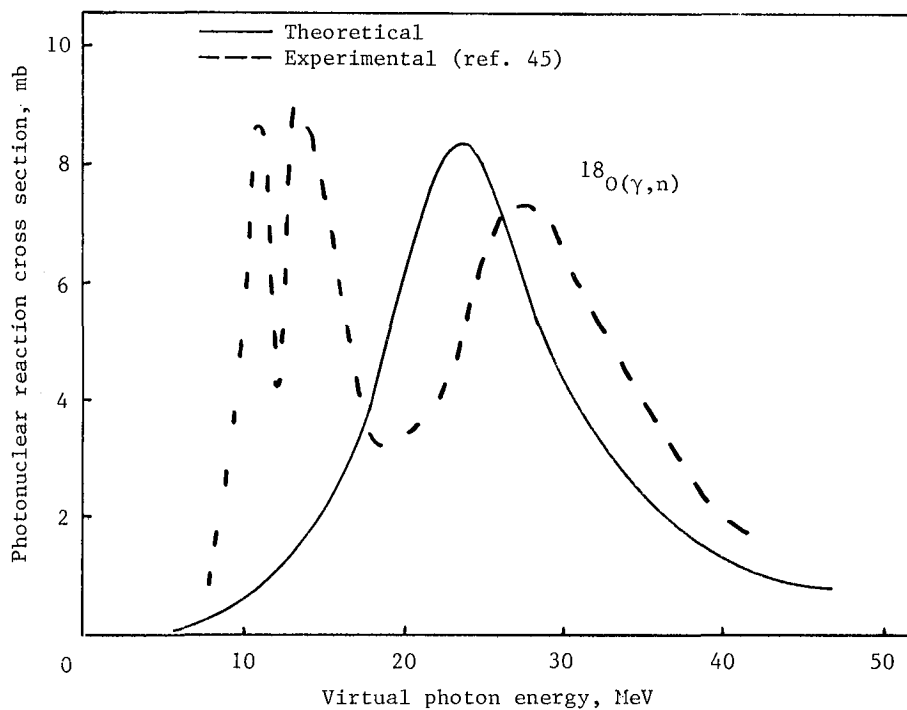
Figure 20.- Theoretical and experimental photoneutron reaction cross section for
^{18}O. Width, Γ = 12 MeV, and neutron branching ratio, g_n = 0.6, have both
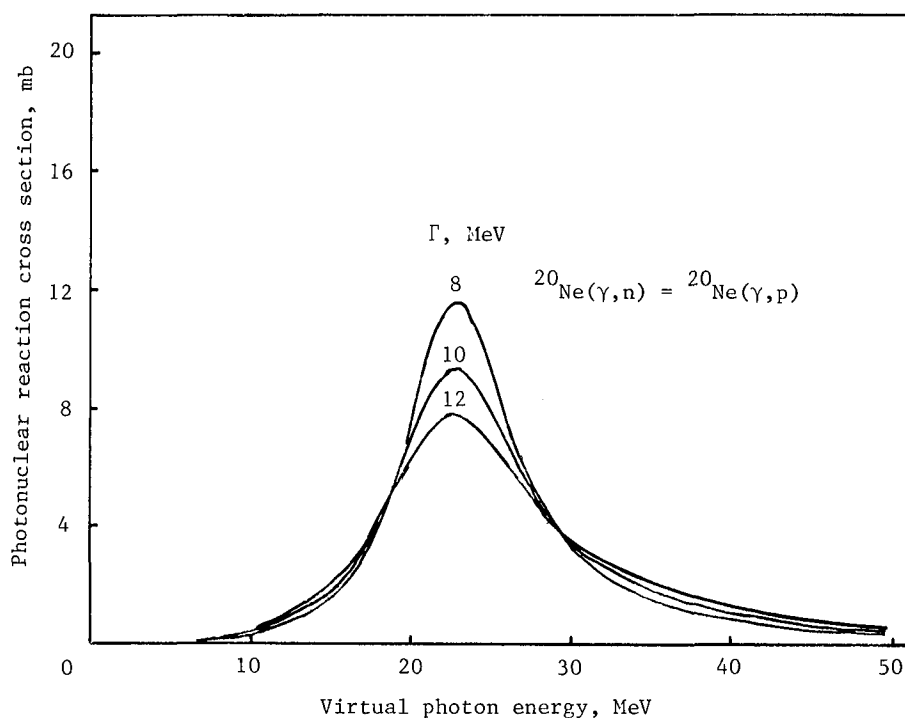been adjusted to fit data.

40
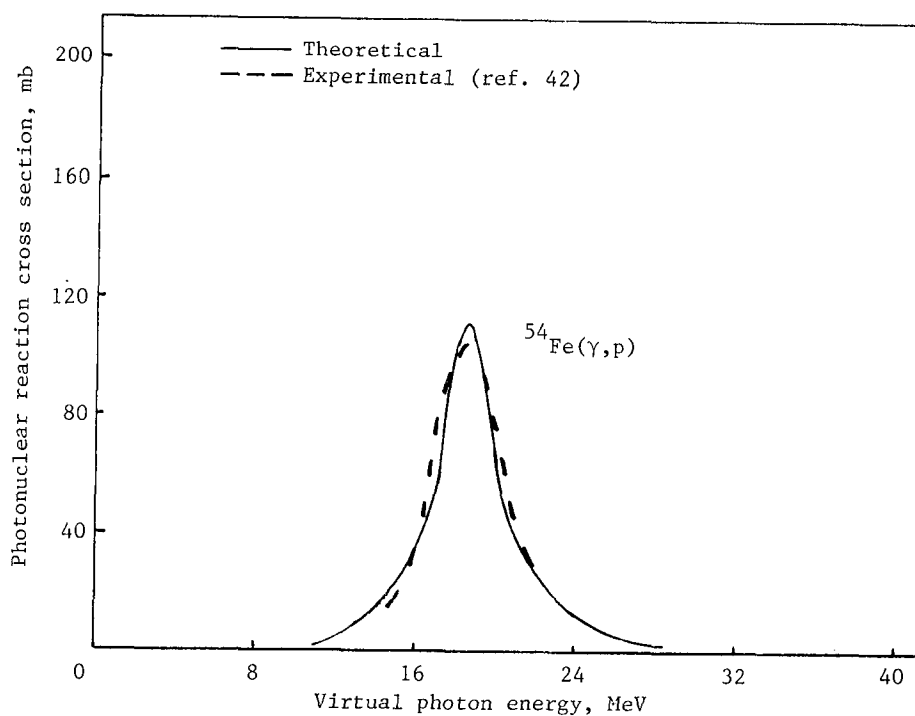
Figure 21.– Theoretical and experimental photoproton reaction cross section for ^{54}Fe. Width, $\Gamma = 3$ MeV, and proton branching ratio, $g_p = 0.7$, have both been adjusted to fit data.

Figure 22.– Theoretical and experimental photoneutron reaction cross section for ^{54}Fe. Width, $\Gamma = 3$ MeV, and neutron branching ratio, $g_n = 0.3$, have both been adjusted to fit data.

Figure 23.- Theoretical photoneutron and photoproton reaction cross sections for ^{20}Ne for various widths. The branching ratios, $g_p = g_n = 0.5$ (table 1), indicate that photoproton and photoneutron cross sections are identical.
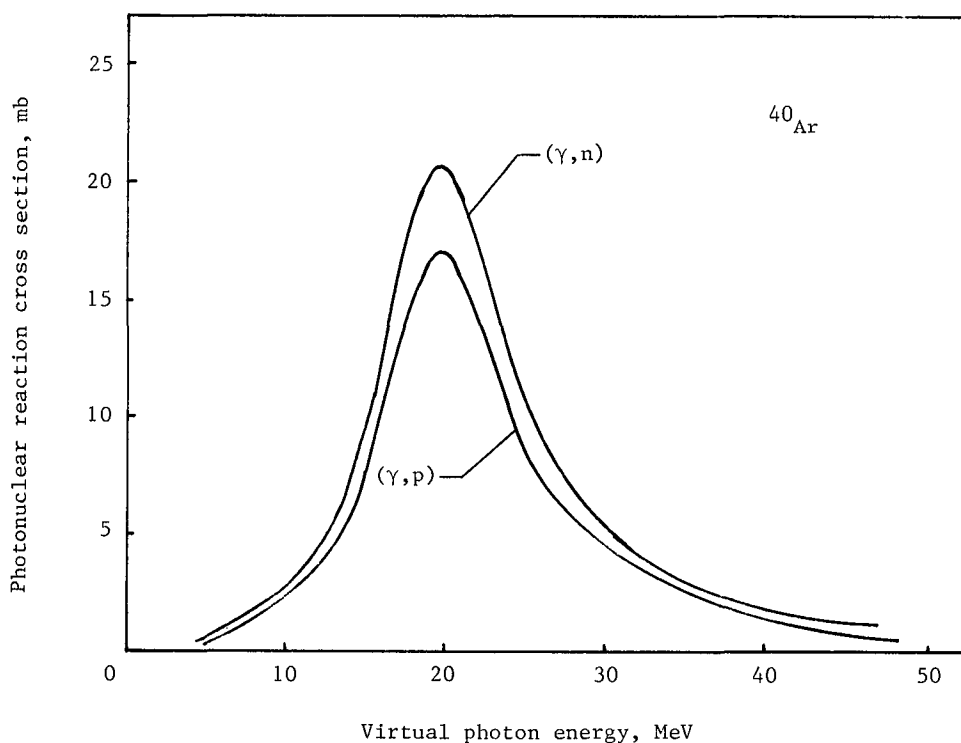
Figure 24.- Theoretical photoneutron and photoproton reaction cross sections for ^{40}Ar. Widths and branching ratios are as in table 1.
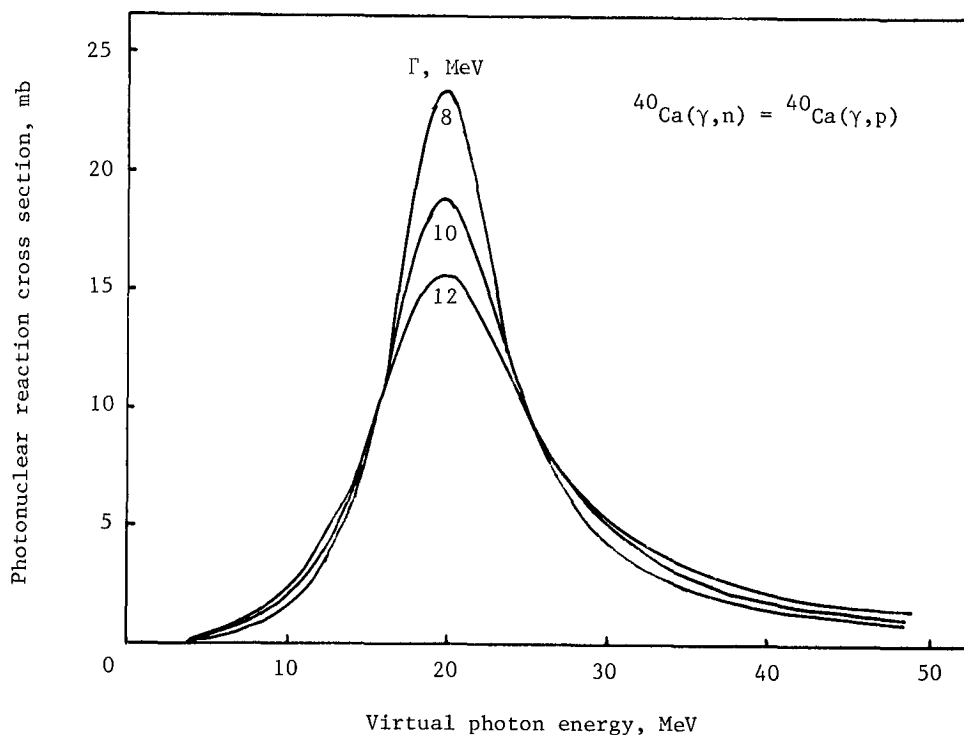
Figure 25.- Theoretical photoneutron and photoproton reaction cross sections for ^{40}Ca. The branching ratios, $g_p = g_n = 0.5$ (table 1), indicate that photoproton and photoneutron cross sections are identical.
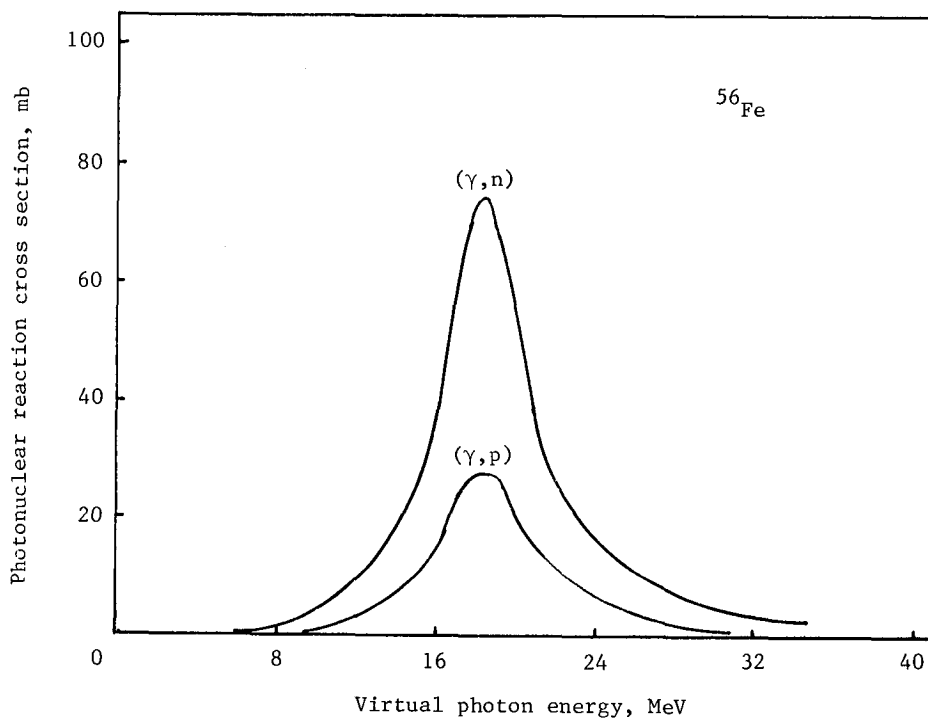

Figure 26.- Theoretical photoneutron and photoproton reaction cross sections for ^{56}Fe. Width, $\Gamma = 5$ MeV, is taken from Westfall et al. (ref. 27) and branching ratios are as in table 1.
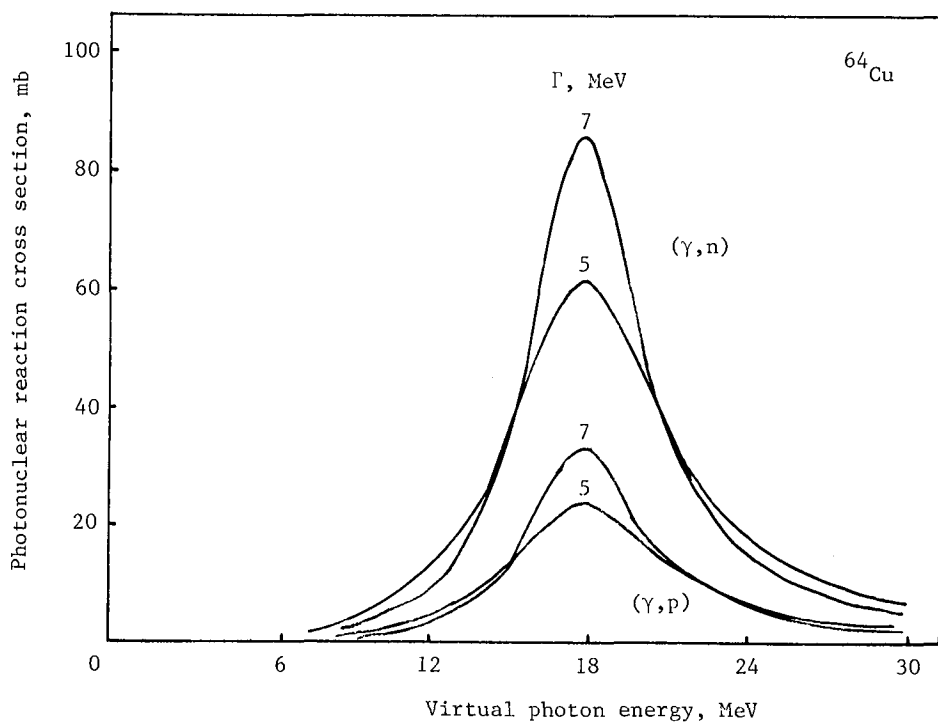
Figure 27.- Theoretical photoneutron and photoproton reaction cross sections for ^{64}Cu for various widths. Branching ratios are as in table 1.
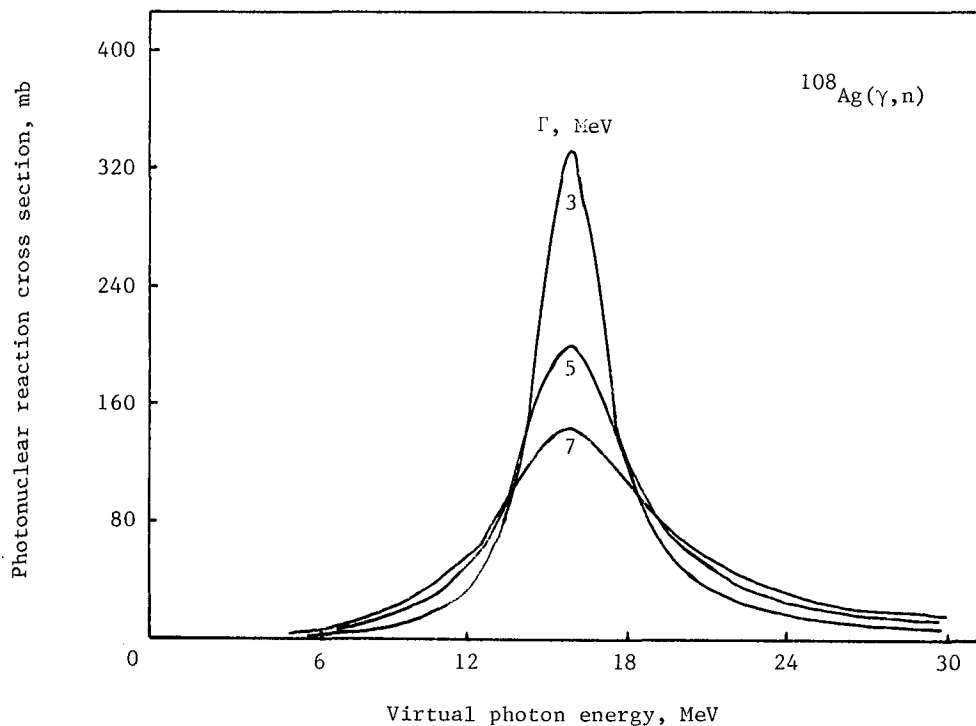

Figure 28.- Theoretical photoneutron reaction cross section for ^{108}Ag. Photoproton cross section is negligible; i.e., $g_p \approx 0$ (ref. 44).

1. Report No. NASA TP-2527	2. Government Accession No.	3. Recipient's Catalog No.
4. Title and Subtitle Electromagnetic Dissociation Effects in Galactic Heavy-Ion Fragmentation		5. Report Date February 1986
		6. Performing Organization Code 199-22-76-01
7. Author(s) John W. Norbury and Lawrence W. Townsend		8. Performing Organization Report No. L-16033
		10. Work Unit No.
9. Performing Organization Name and Address NASA Langley Research Center Hampton, VA 23665-5225		11. Contract or Grant No.
		13. Type of Report and Period Covered Technical Paper
12. Sponsoring Agency Name and Address National Aeronautics and Space Administration Washington, DC 20546-0001		
		14. Sponsoring Agency Code

15. Supplementary Notes

16. Abstract

Methods for calculating cross sections for the breakup of galactic heavy ions by the Coulomb fields of the interacting nuclei are presented. By using the Weizsäcker-Williams method of virtual quanta, estimates of electromagnetic dissociation cross sections for a variety of reactions applicable to galactic cosmic ray shielding studies are presented and compared with other predictions and with available experimental data.

17. Key Words (Suggested by Author(s)) Coulomb dissociation Heavy-ion fragmentation Galactic cosmic ray shielding	18. Distribution Statement Unclassified – Unlimited Subject Category 73		
19. Security Classif. (of this report) Unclassified	20. Security Classif. (of this page) Unclassified	21. No. of Pages 45	22. Price A03

National Aeronautics and
Space Administration
Code NIT-4

Washington, D.C.
20546-0001

To
Library
M/S 185

NASA